Global seismic tomography using teleseismic and core-diffracted body waves

Kasra Hosseini, Karin Sigloch and Tarje Nissen-Meyer

Department of Earth Sciences, University of Oxford

Core-diffracted P waves (Pdiff)

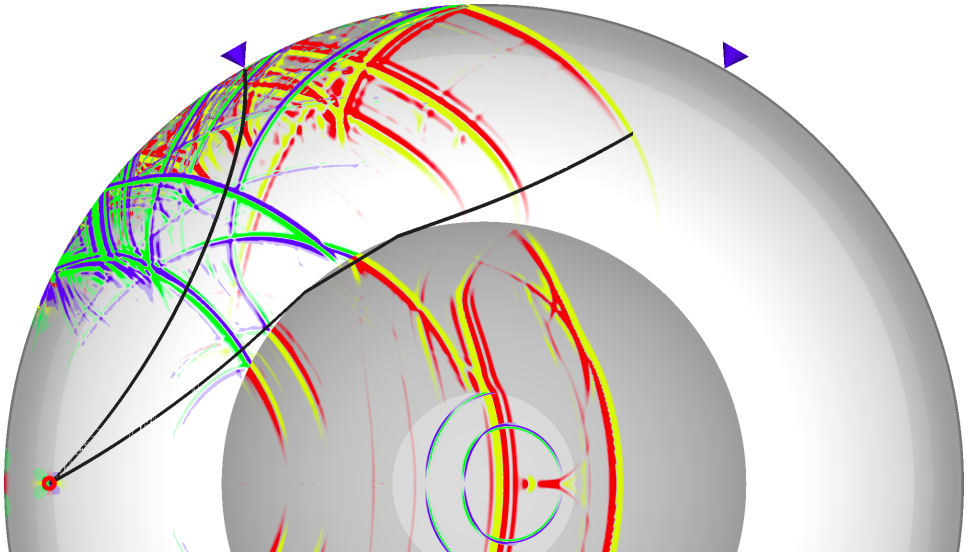

Core-diffracted waves are seismic **body waves** that dive deep enough to **sense the earth's core.**

Core-diffracted P waves (Pdiff)

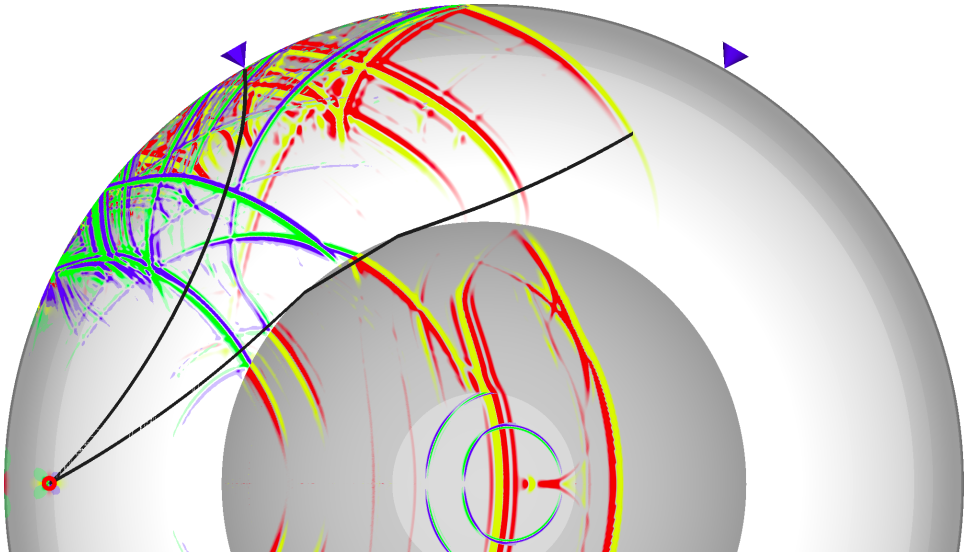

Core-diffracted waves are seismic **body waves** that dive deep enough to **sense the earth's core.**

P-diffracted waves are highly **attenuative** and **dispersive**: the effect of diffraction.

Hosseini and Sigloch, 2015

Core-diffracted P waves (Pdiff)

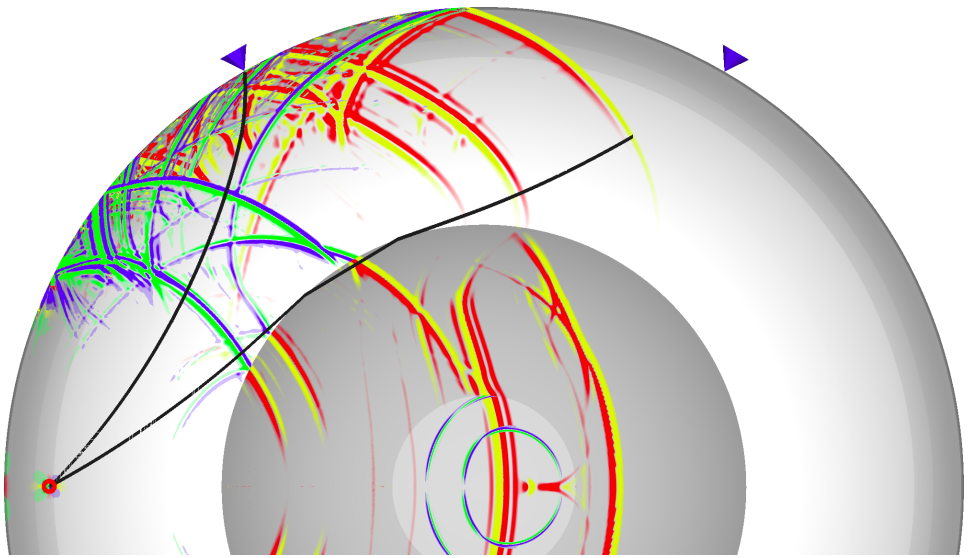

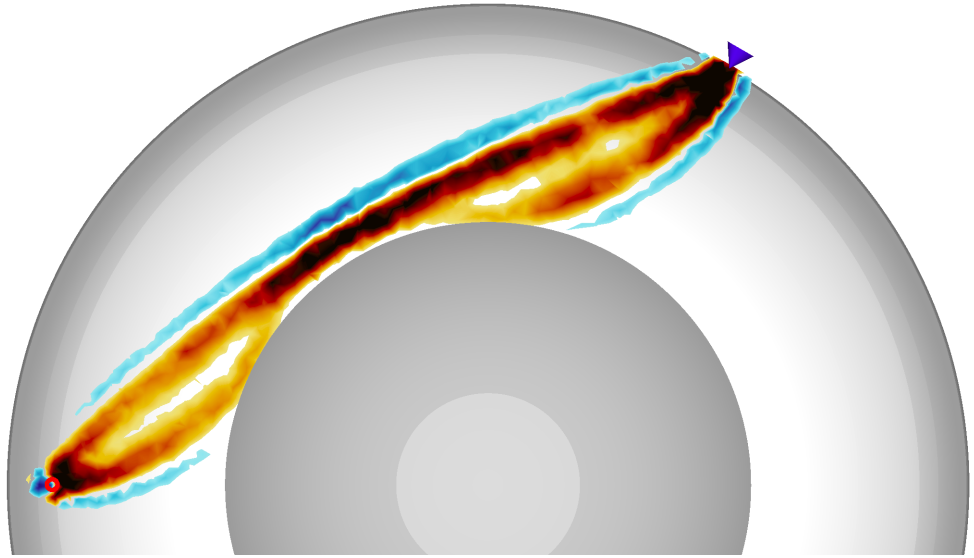

Core-diffracted waves are seismic **body waves** that dive deep enough to **sense the earth's core.**

P-diffracted waves are highly **attenuative** and **dispersive**: the effect of diffraction.

Ray theory is a poor approximation of the true, finite-frequency sensitivity of a core-diffracted wave.

Hosseini and Sigloch, 2015

Multifrequency measurement

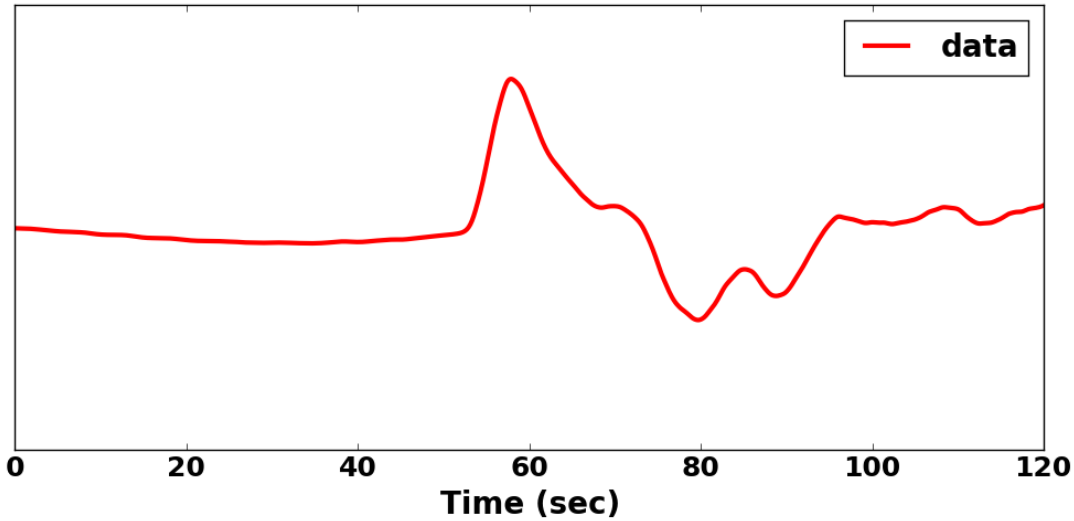

Multifrequency measurement

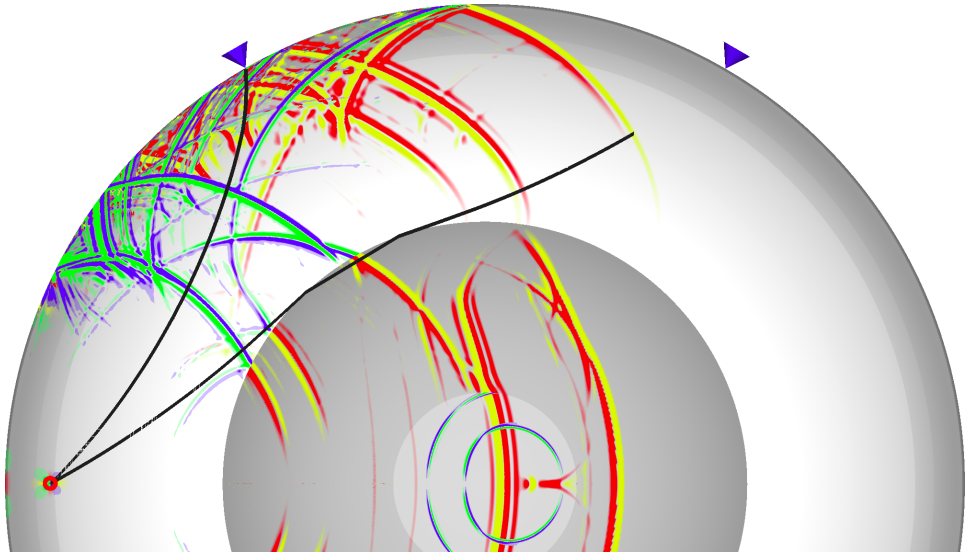

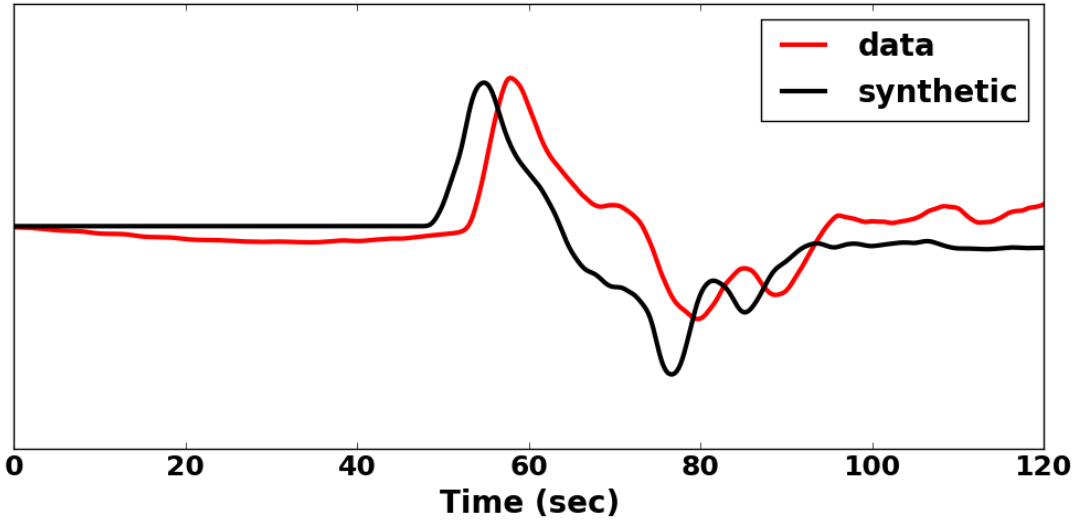

Multifrequency measurement

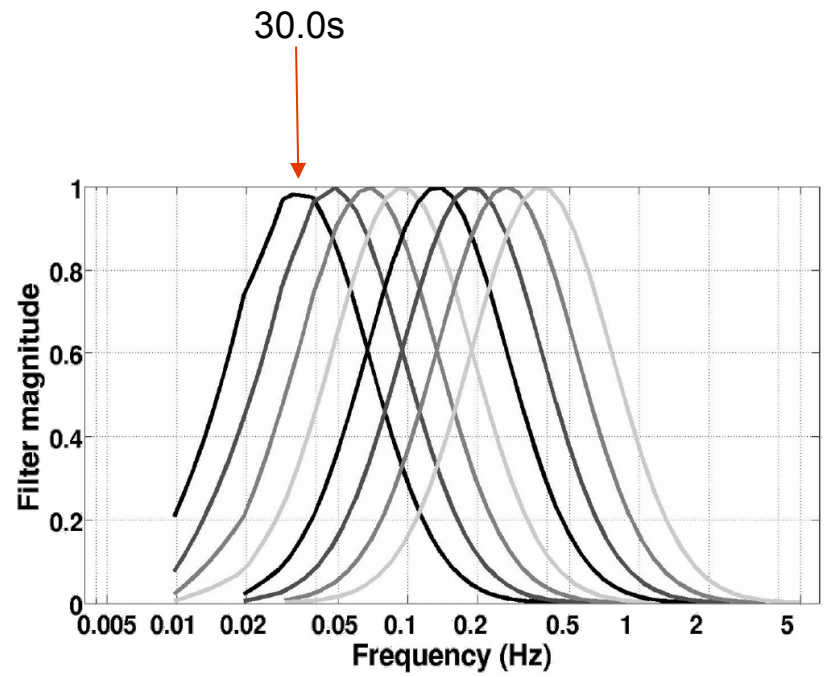

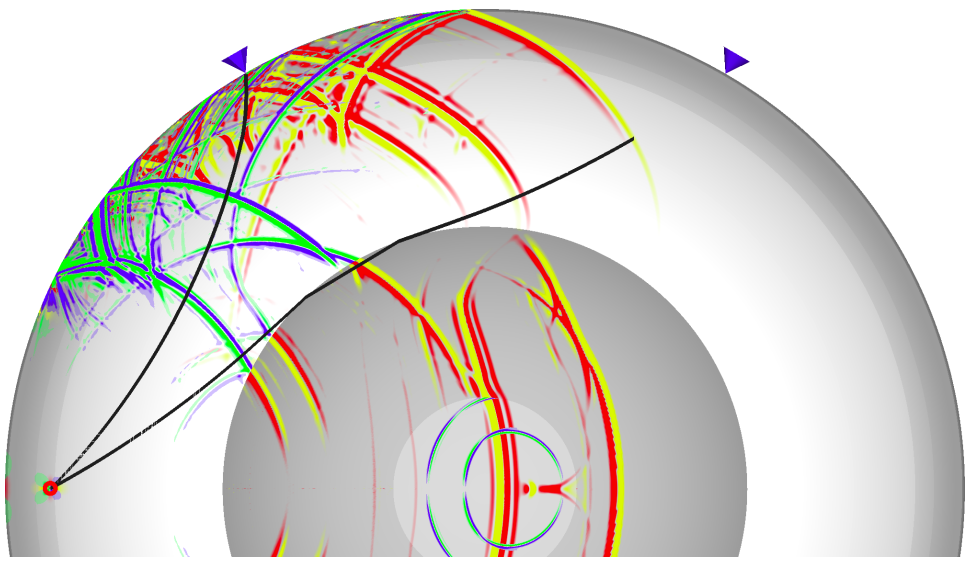

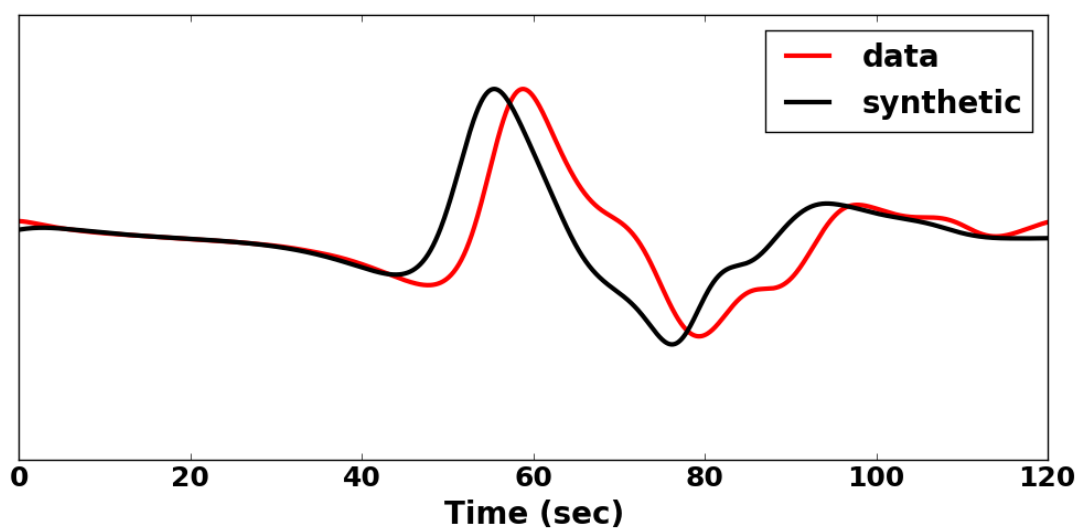

Multifrequency measurement

Compute the cross-correlation function between bandpassed observed (data) and **predicted waveforms (synthetic)** in each passband.

Gabor filters with Center periods:
30.0 to 2.7 s (0.033 to 0.37 Hz).

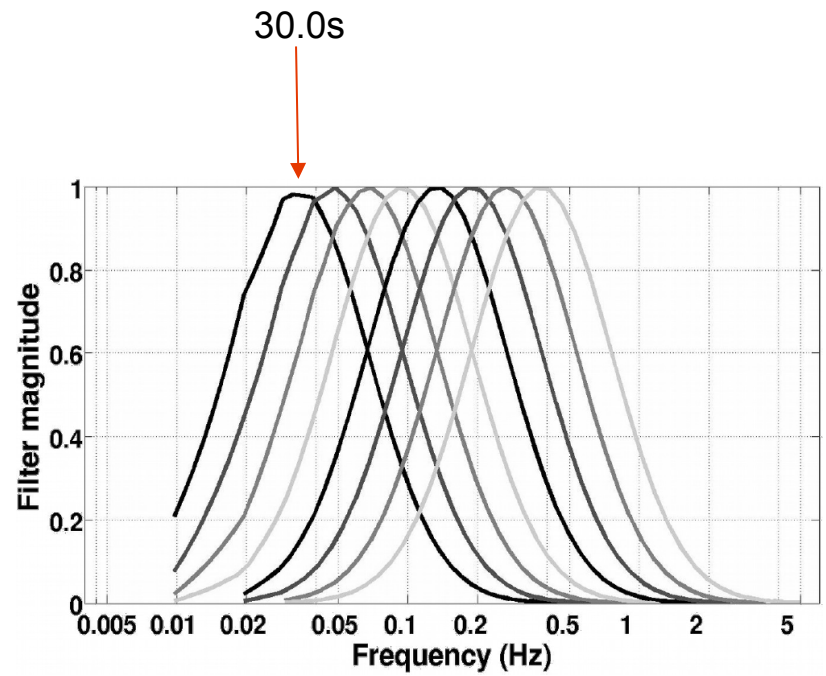

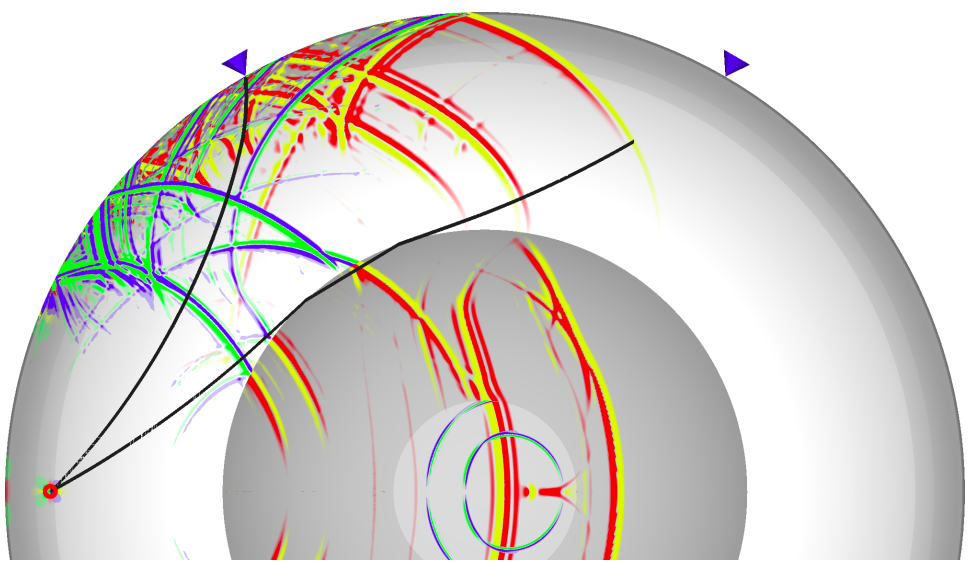

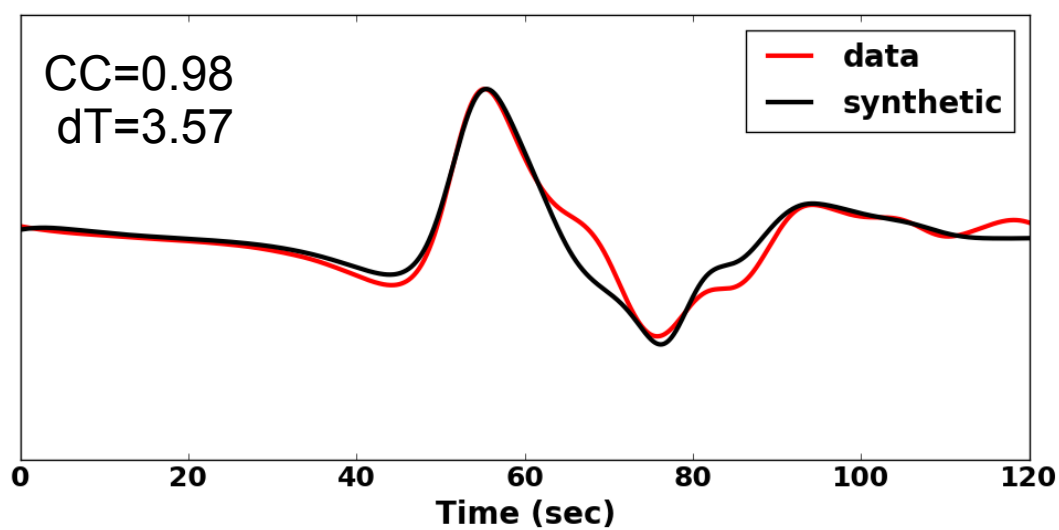

Multifrequency measurement

Compute the cross-correlation function between bandpassed observed (data) and **predicted waveforms (synthetic)** in each passband.

Gabor filters with Center periods:
30.0 to 2.7 s (0.033 to 0.37 Hz).

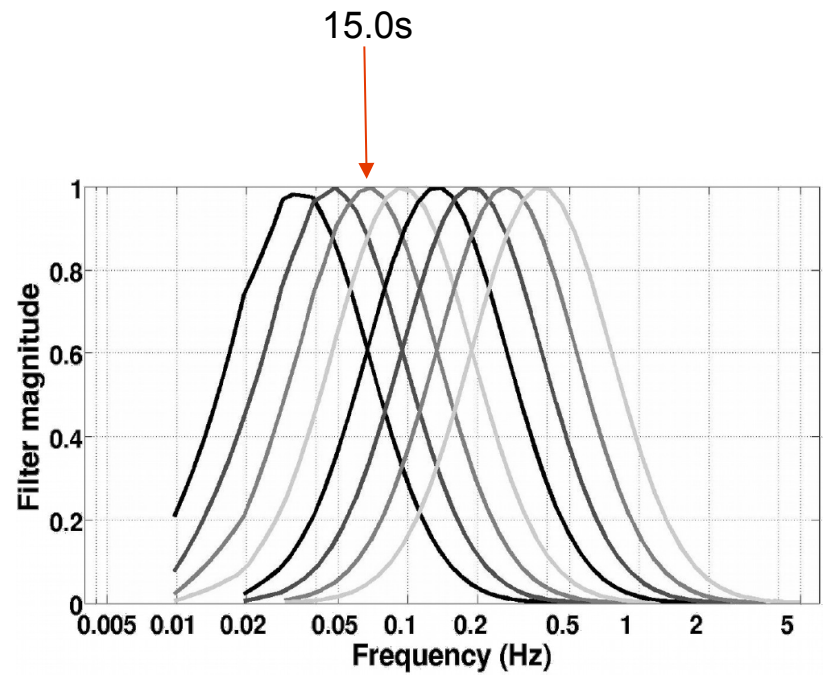

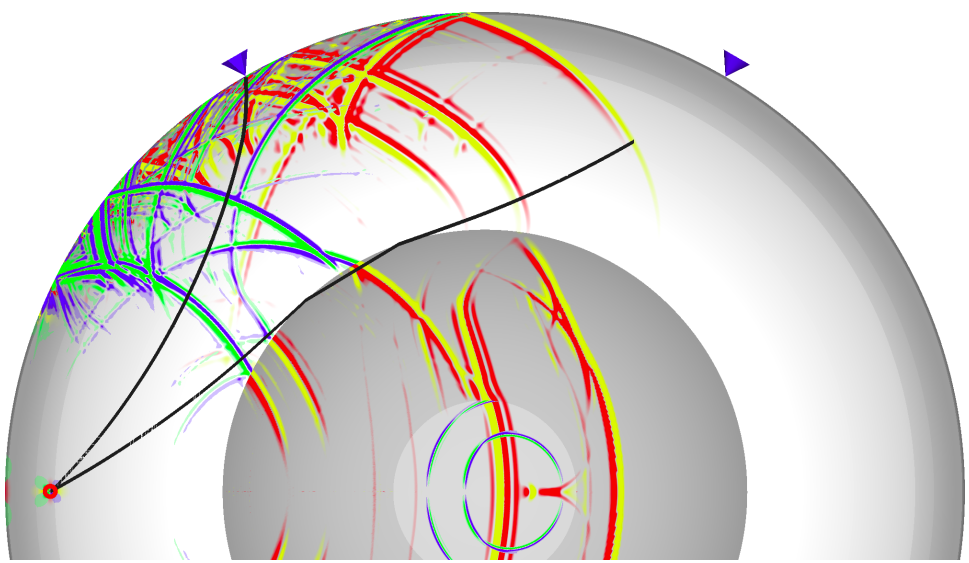

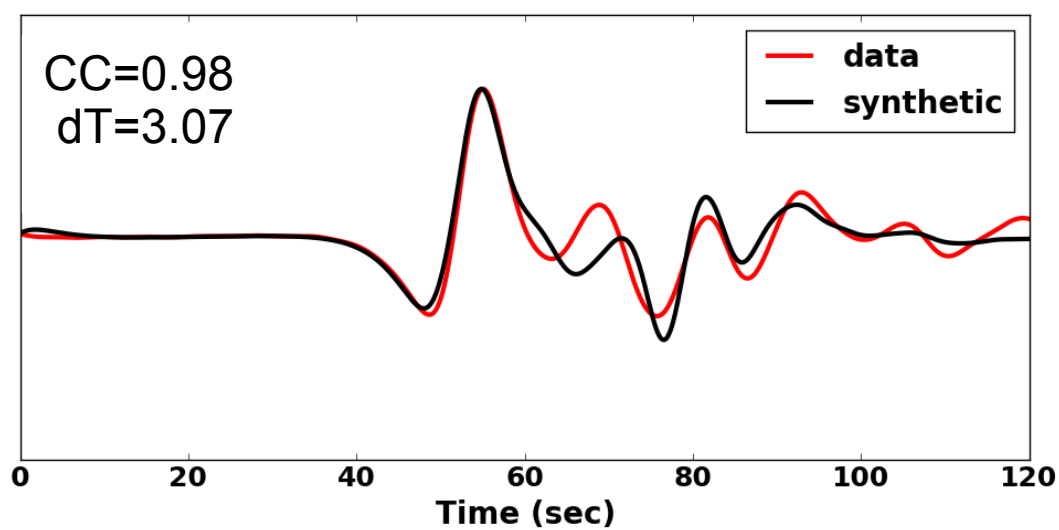

Multifrequency measurement

Compute the cross-correlation function between bandpassed observed (data) and **predicted waveforms (synthetic)** in each passband.

Gabor filters with Center periods:
30.0 to 2.7 s (0.033 to 0.37 Hz).

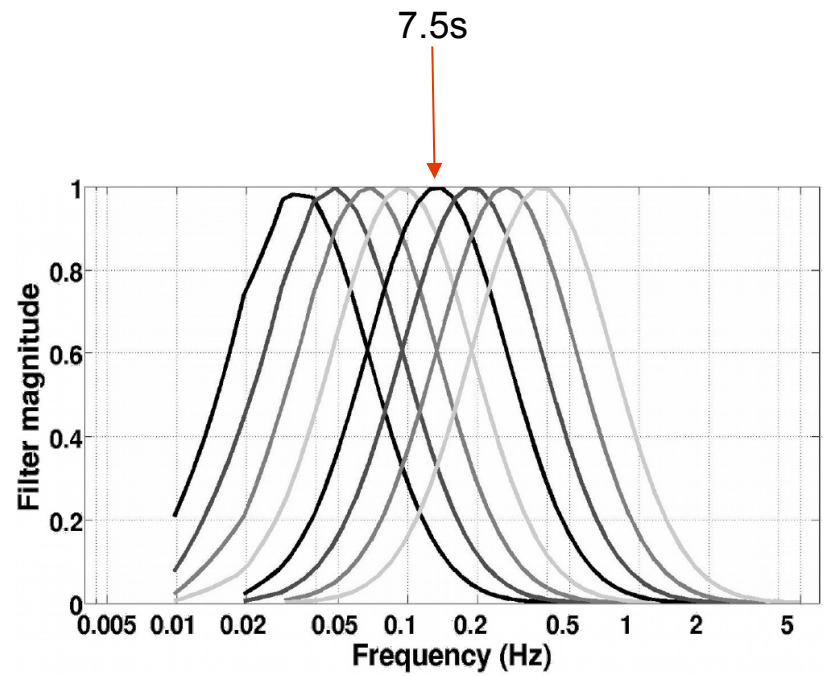

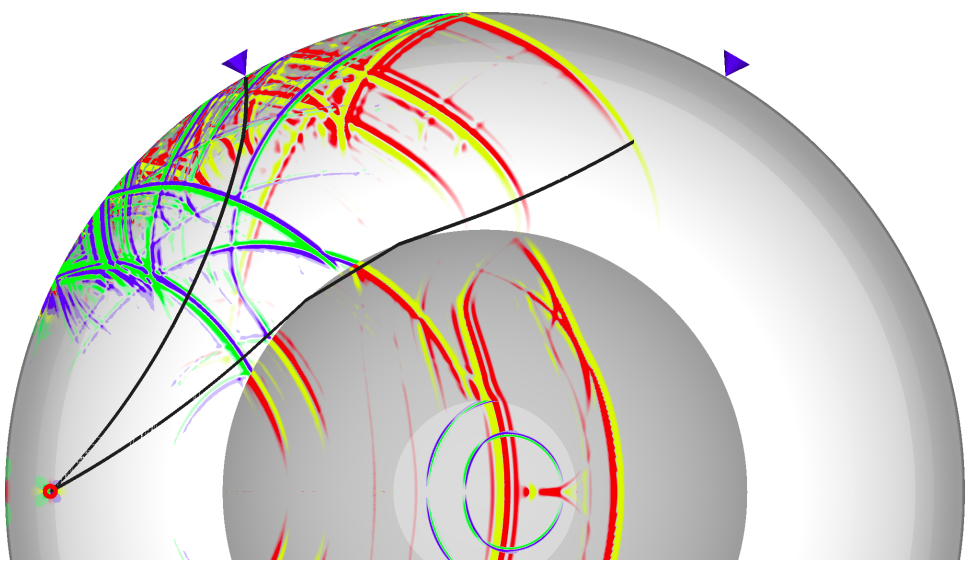

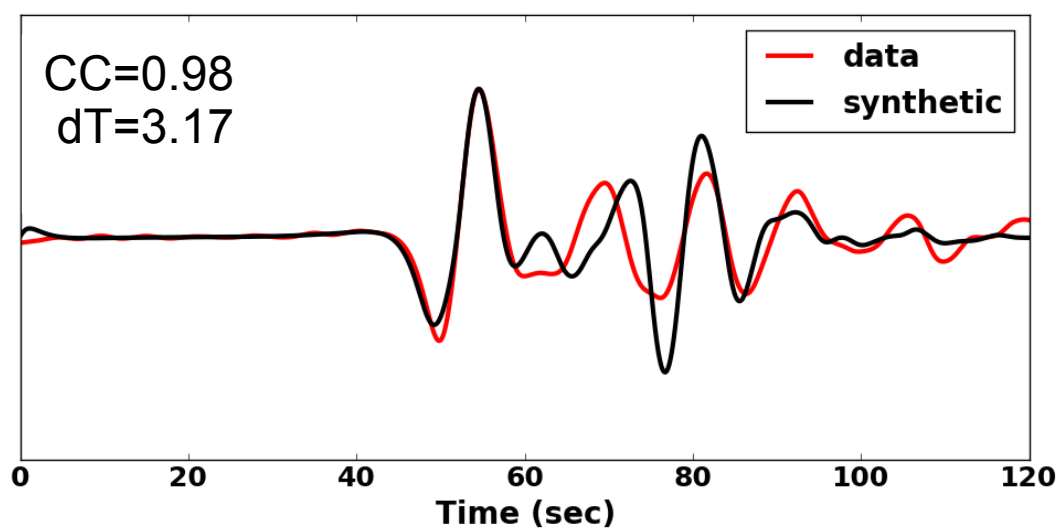

Global dataset

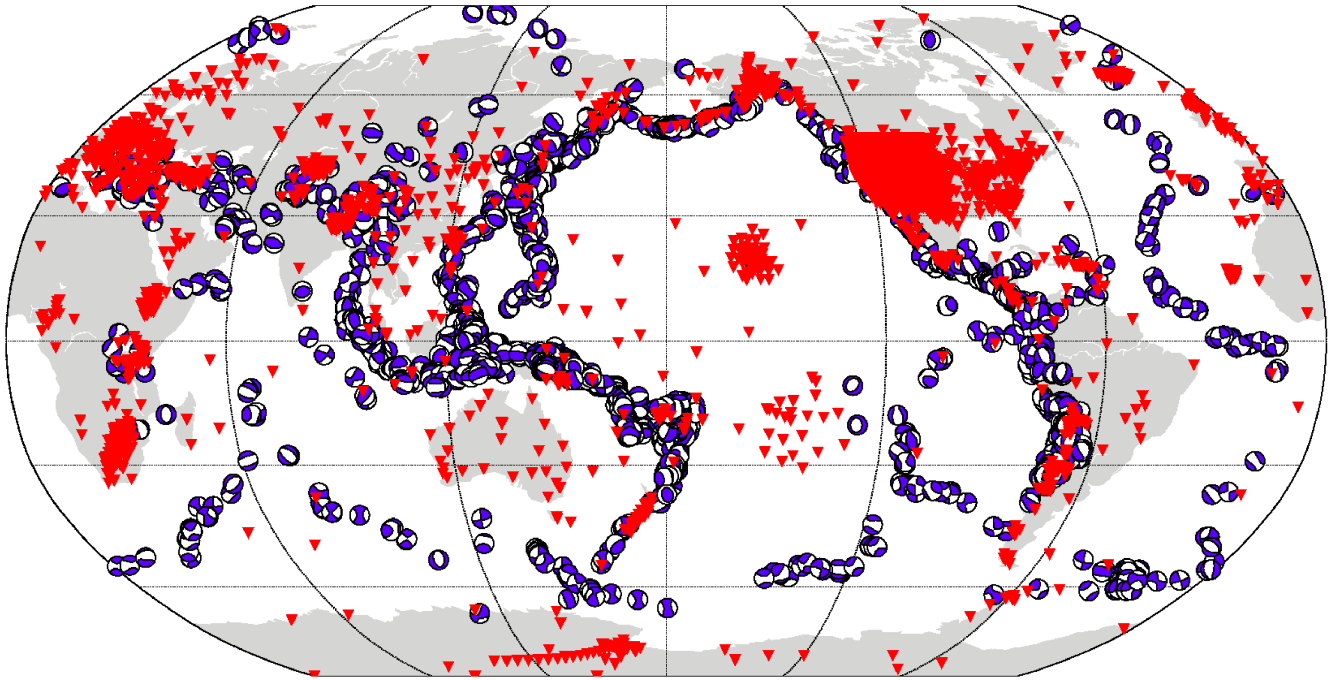

Global distribution of **1857 earthquake** sources and **4085 broad-band receivers**.

Combination of **P, PP and Pdiff** covers a wide range of mantle **depths** and **distances**.

Hosseini and Sigloch, 2015

Global dataset

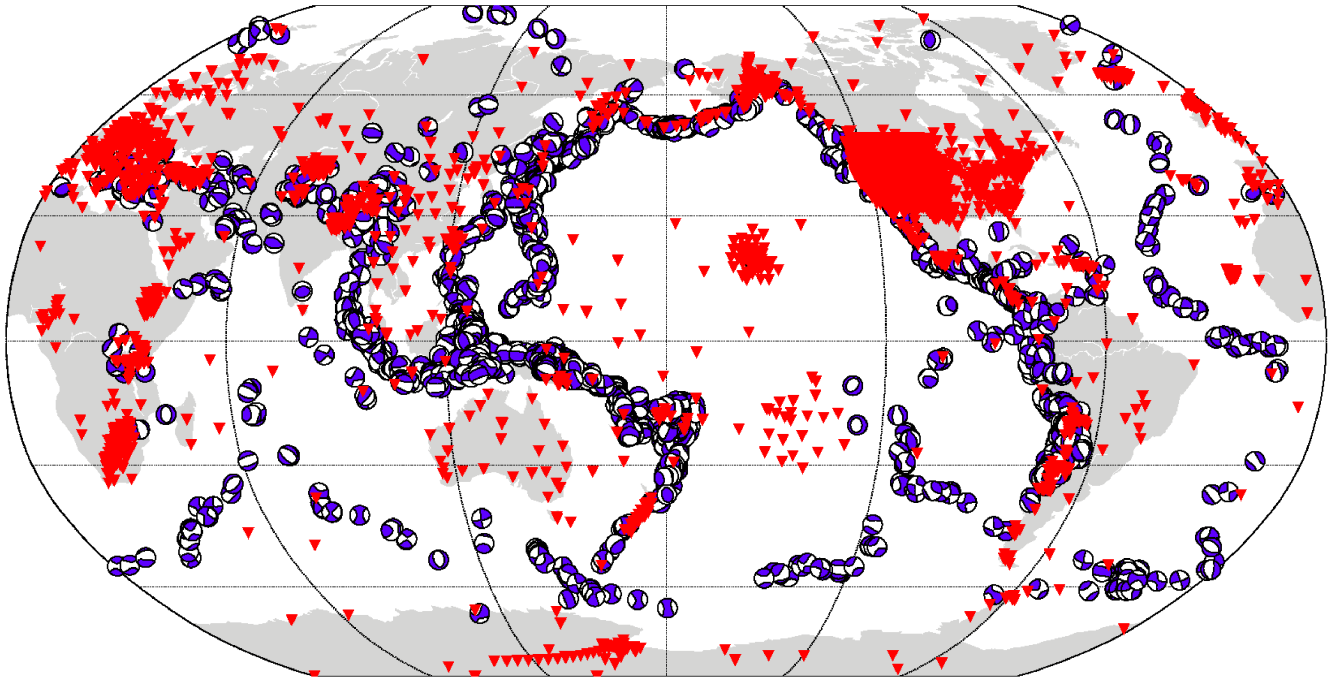

Global distribution of **1857 earthquake** sources and **4085 broad-band receivers**.

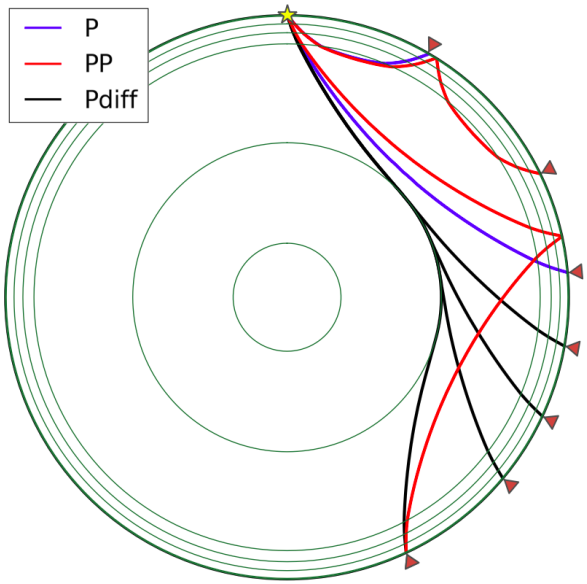

Combination of **P, PP and Pdiff** covers a wide range of mantle **depths** and **distances**.

Hosseini and Sigloch, 2015

P, PP and Pdiff sensitivity kernels

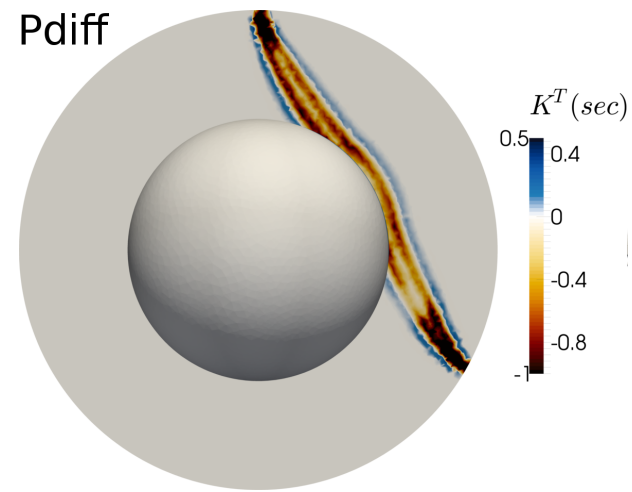

3-D sensitivity kernels of **P, PP and Pdiff** using Dahlen et al. (2000).

<u>Frequency-dependent</u>: calculated for the **bandpass filters** used for traveltime measurements.

Pdiff kernels are approximated as Dahlen's method can not account for diffraction.

P, PP and Pdiff sensitivity kernels

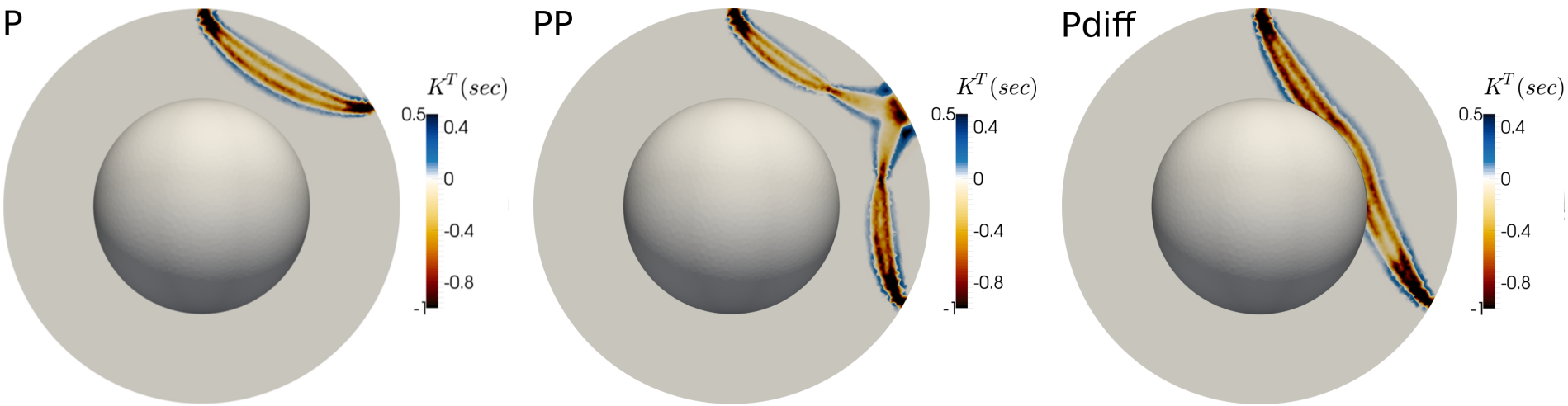

3-D sensitivity kernels of **P, PP and Pdiff** using Dahlen et al. (2000).

<u>Frequency-dependent</u>: calculated for the **bandpass filters** used for traveltime measurements.

Pdiff kernels are approximated as Dahlen's method can not account for diffraction.

P, PP and Pdiff sensitivity kernels

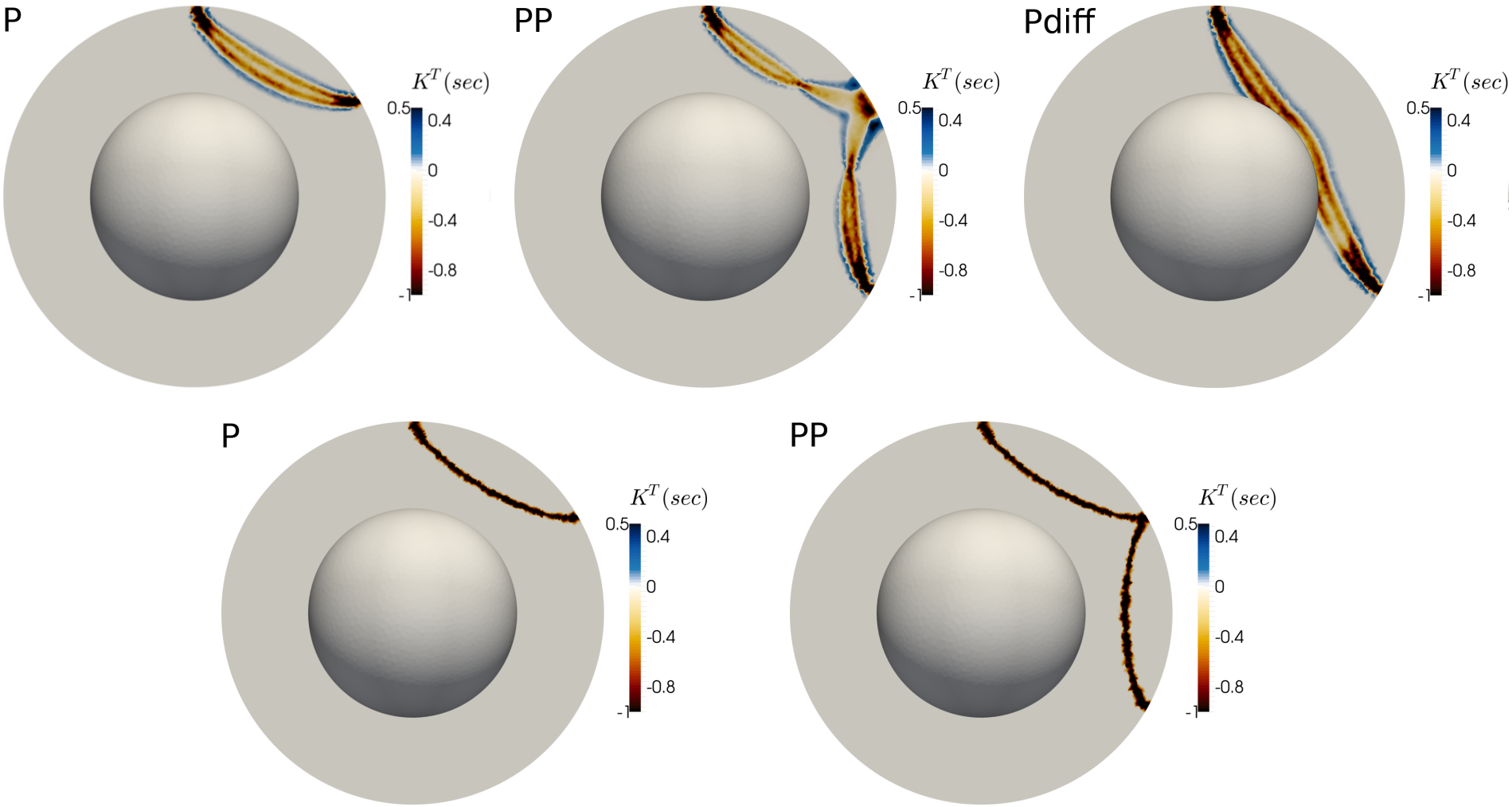

3-D sensitivity kernels of **P, PP and Pdiff** using Dahlen et al. (2000).

<u>Frequency-dependent</u>: calculated for the **bandpass filters** used for traveltime measurements.

Pdiff kernels are approximated as Dahlen's method can not account for diffraction.

Kernel coverage

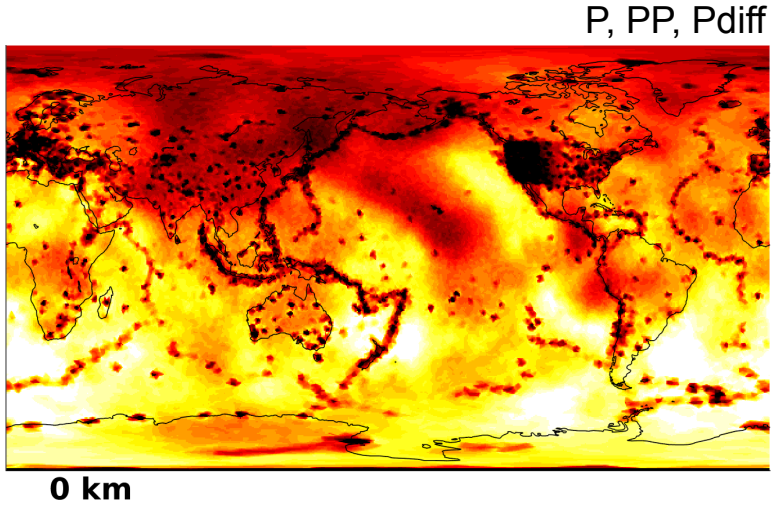

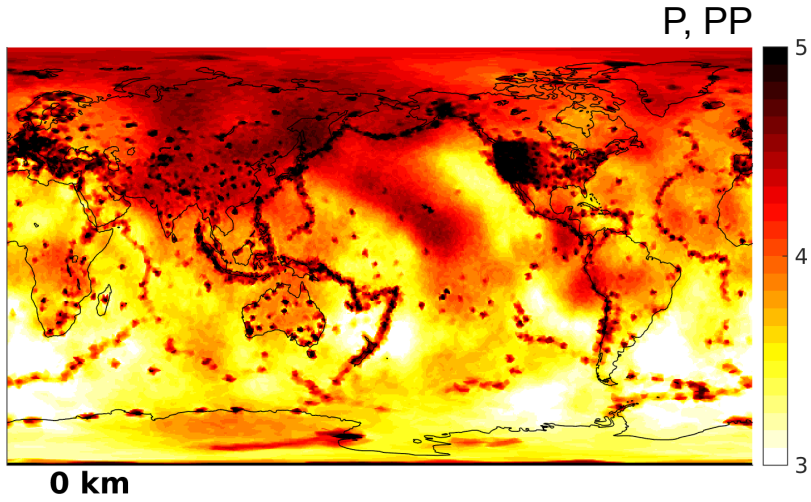

Kernel coverage

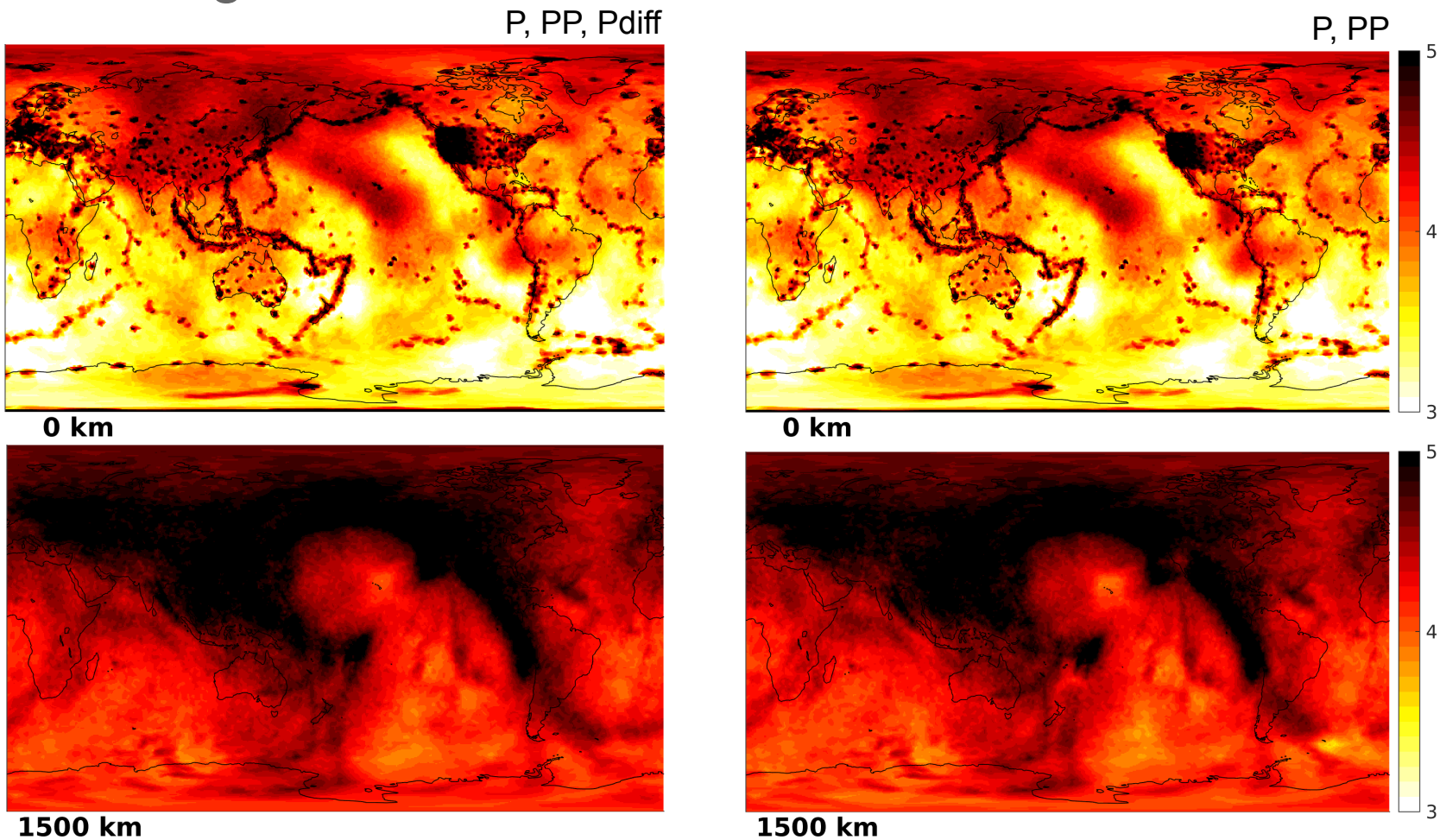

Kernel coverage

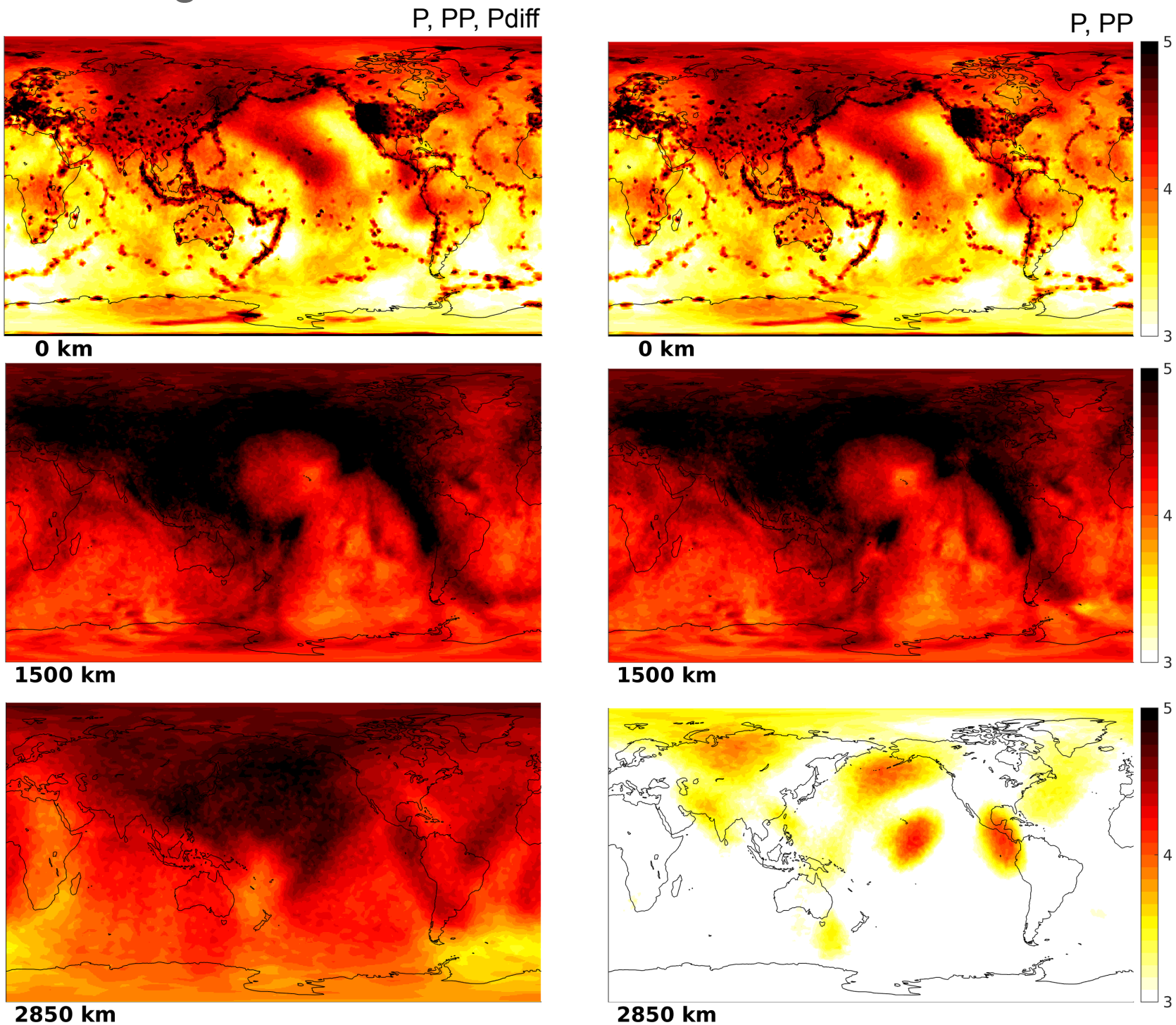

Kernel coverage

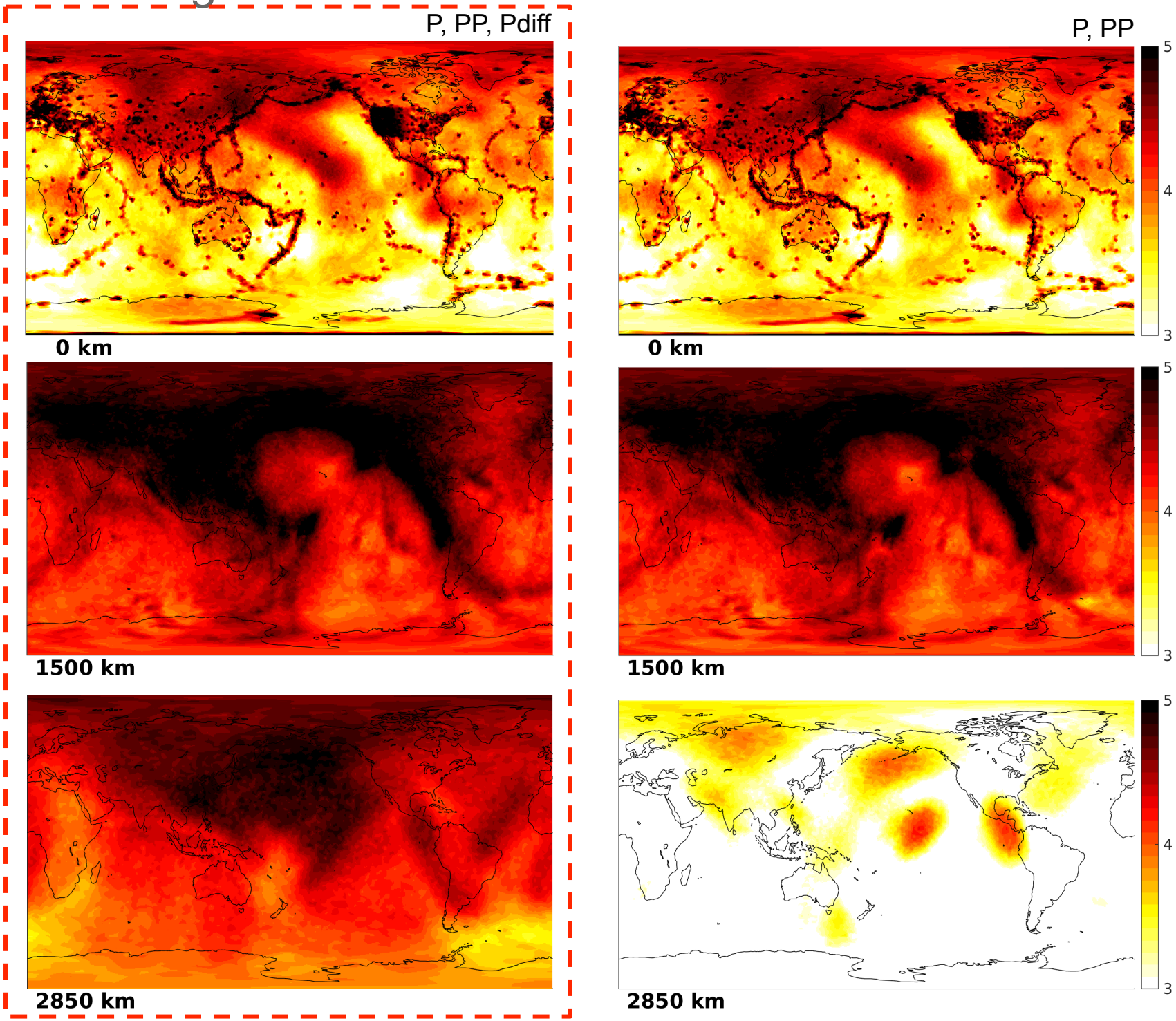

Lowermost mantle structure (2850 km)

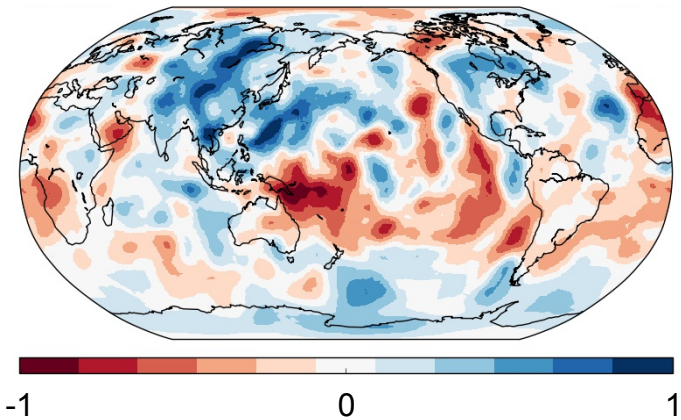

This study (Hosseini et al., 2017 [in prep.])
2.5M multifrequency measurements with dominant periods from 30.0 to 2.7 s
3.4M picked arrival times from EHB catalogue

Lowermost mantle structure (2850 km)

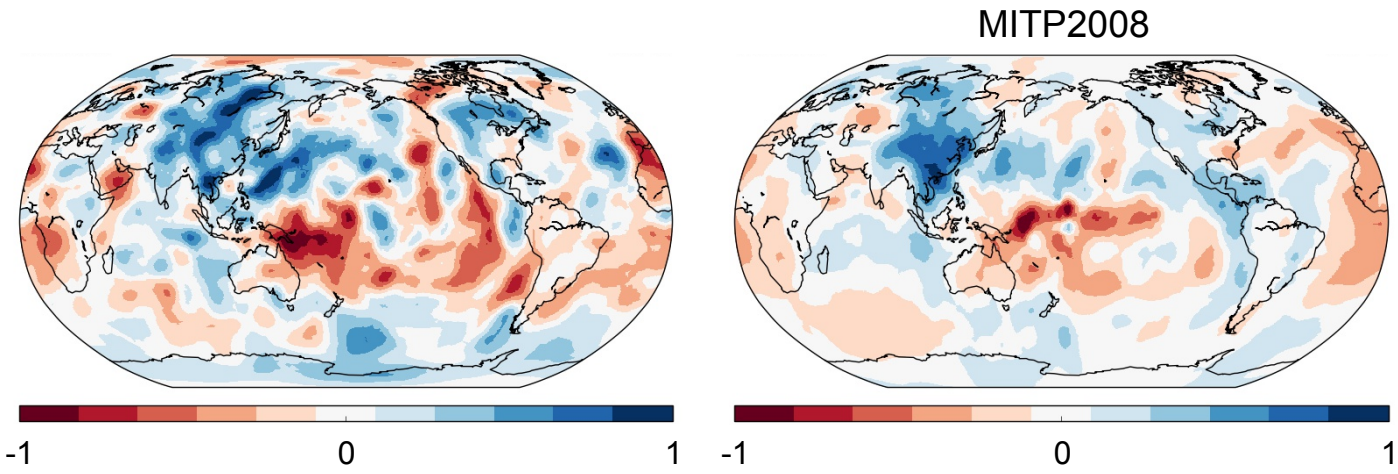

This study (Hosseini et al., 2017 [in prep.])
2.5M multifrequency measurements with dominant periods from 30.0 to 2.7 s
3.4M picked arrival times from EHB catalogue

MIT-P08 (Li et al., 2008)
21K cross-correlation measurements
15.2M picked arrival times with 4.1M composite rays

Lowermost mantle structure (2850 km)

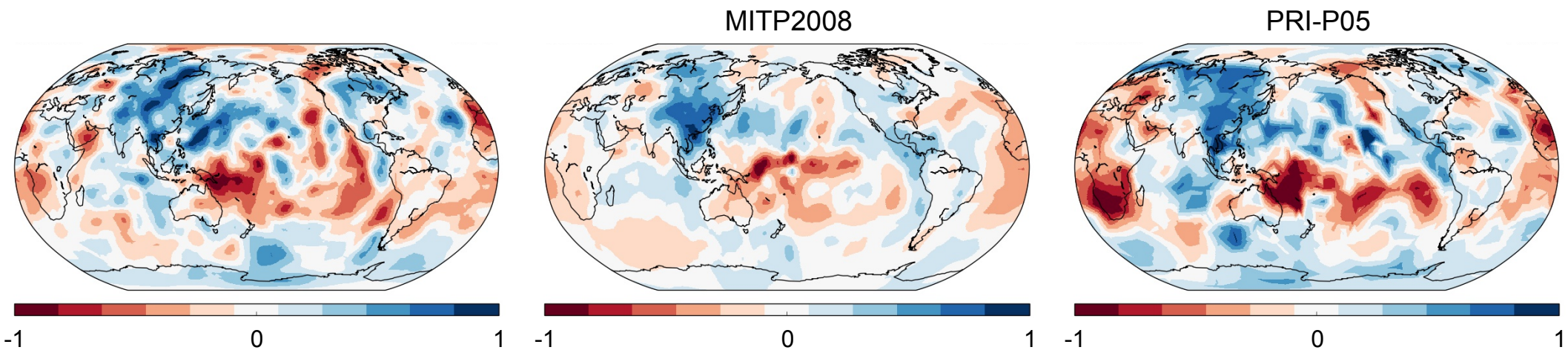

This study (Hosseini et al., 2017 [in prep.])
2.5M multifrequency measurements with dominant periods from 30.0 to 2.7 s
3.4M picked arrival times from EHB catalogue

MIT-P08 (Li et al., 2008)
21K cross-correlation measurements
15.2M picked arrival times with 4.1M composite rays

PRI-P05 (Montelli et al., 2006)
90K finite frequency measurements with 20 s dominant period
1.5M short-period traveltimes from bulletins

Lowermost mantle structure (2850 km)

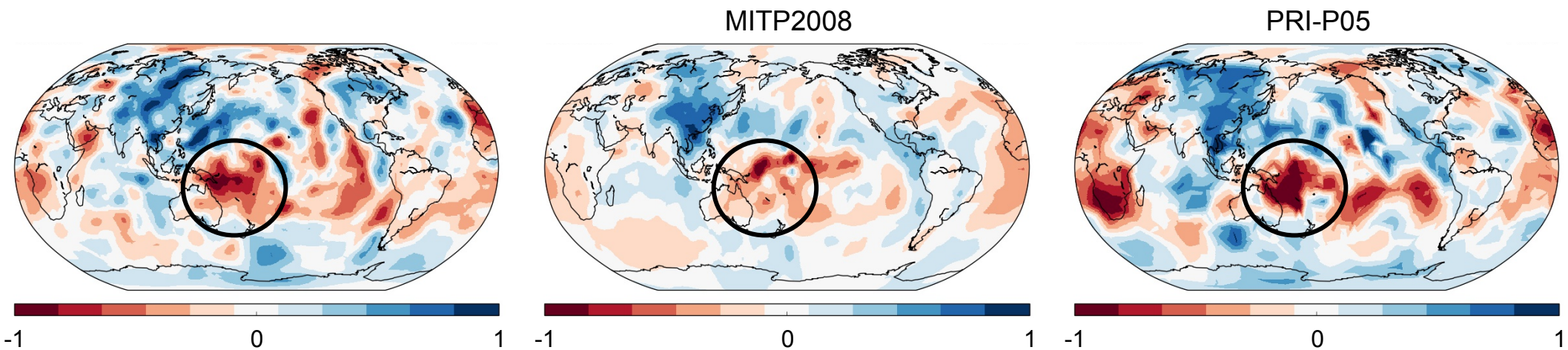

This study (Hosseini et al., 2017 [in prep.])
2.5M multifrequency measurements with dominant periods from 30.0 to 2.7 s
3.4M picked arrival times from EHB catalogue

MIT-P08 (Li et al., 2008)
21K cross-correlation measurements
15.2M picked arrival times with 4.1M composite rays

PRI-P05 (Montelli et al., 2006)
90K finite frequency measurements with 20 s dominant period
1.5M short-period traveltimes from bulletins

Lowermost mantle structure (2850 km)

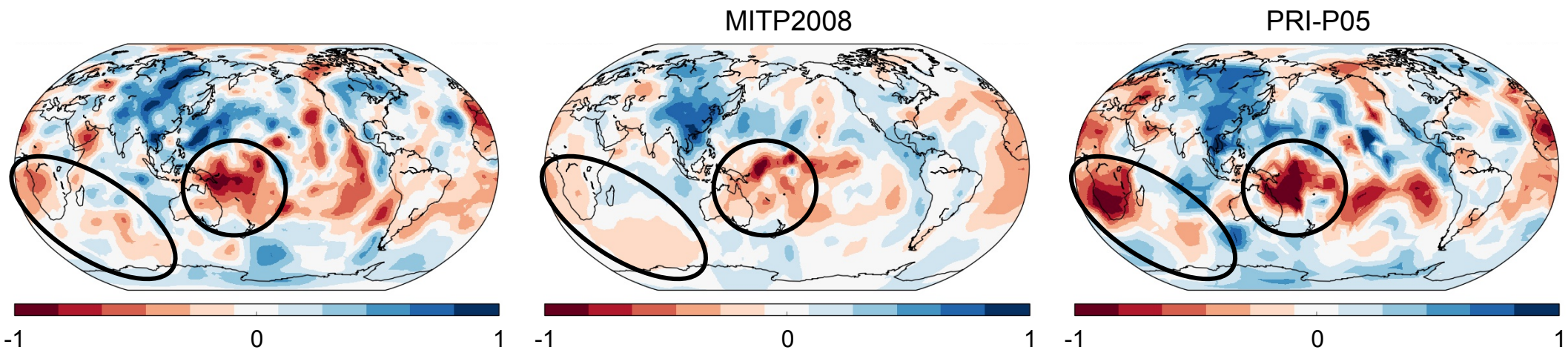

This study (Hosseini et al., 2017 [in prep.])
2.5M multifrequency measurements with dominant periods from 30.0 to 2.7 s
3.4M picked arrival times from EHB catalogue

MIT-P08 (Li et al., 2008)
21K cross-correlation measurements
15.2M picked arrival times with 4.1M composite rays

PRI-P05 (Montelli et al., 2006)
90K finite frequency measurements with 20 s dominant period
1.5M short-period traveltimes from bulletins

Lowermost mantle structure (2850 km)

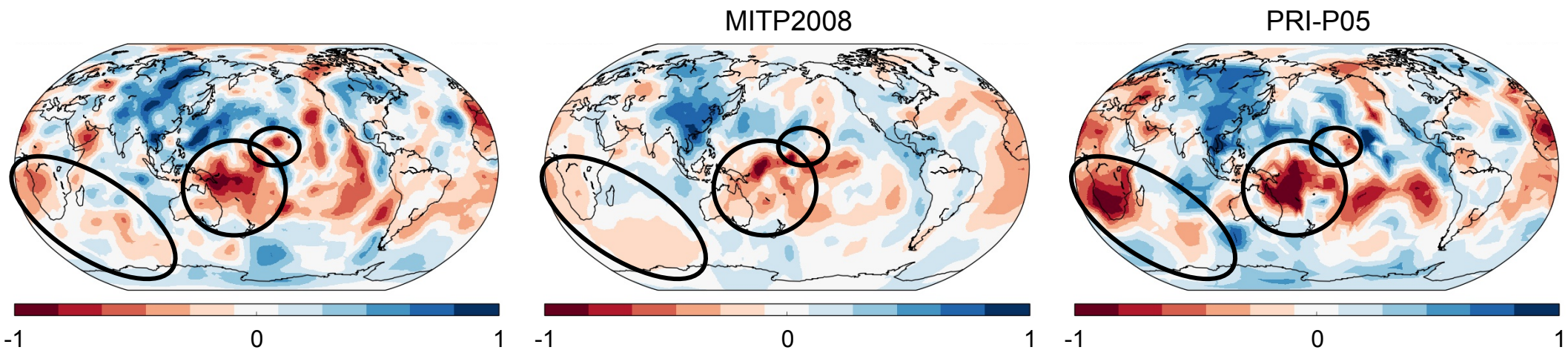

This study (Hosseini et al., 2017 [in prep.])
2.5M multifrequency measurements with dominant periods from 30.0 to 2.7 s
3.4M picked arrival times from EHB catalogue

MIT-P08 (Li et al., 2008)
21K cross-correlation measurements
15.2M picked arrival times with 4.1M composite rays

PRI-P05 (Montelli et al., 2006)
90K finite frequency measurements with 20 s dominant period
1.5M short-period traveltimes from bulletins

Lowermost mantle structure (2850 km)

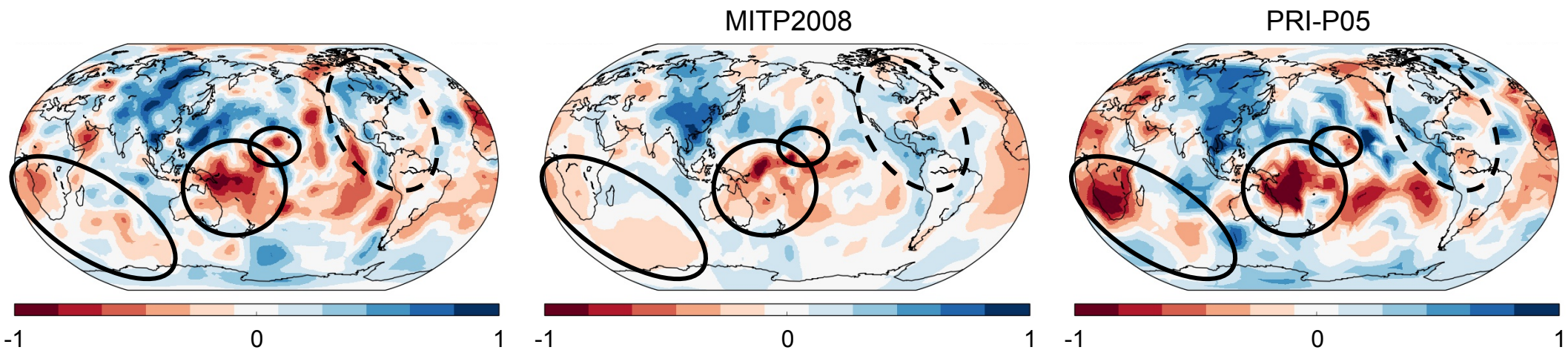

This study (Hosseini et al., 2017 [in prep.])
2.5M multifrequency measurements with dominant periods from 30.0 to 2.7 s
3.4M picked arrival times from EHB catalogue

MIT-P08 (Li et al., 2008)
21K cross-correlation measurements
15.2M picked arrival times with 4.1M composite rays

PRI-P05 (Montelli et al., 2006)
90K finite frequency measurements with 20 s dominant period
1.5M short-period traveltimes from bulletins

Lowermost mantle structure (2850 km)

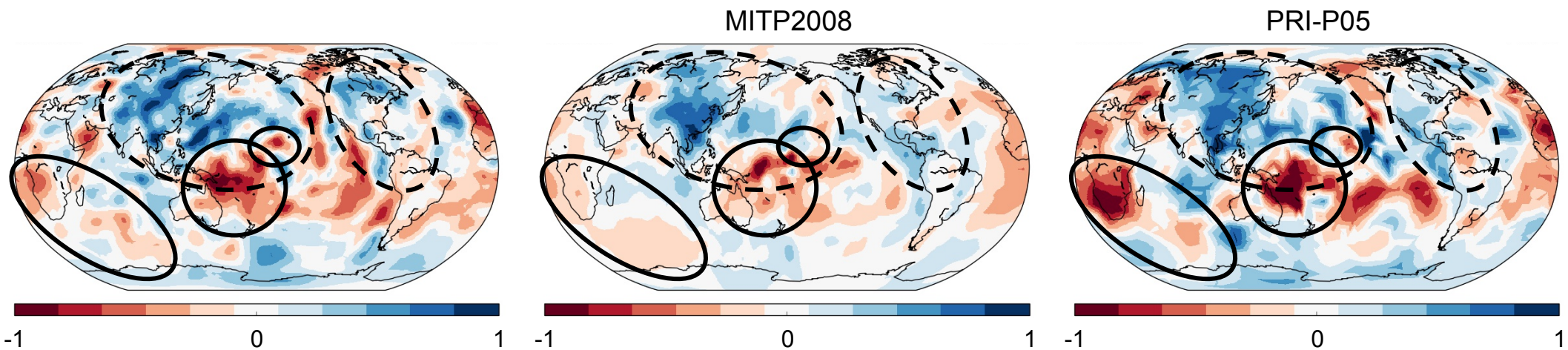

This study (Hosseini et al., 2017 [in prep.])
2.5M multifrequency measurements with dominant periods from 30.0 to 2.7 s
3.4M picked arrival times from EHB catalogue

MIT-P08 (Li et al., 2008)
21K cross-correlation measurements
15.2M picked arrival times with 4.1M composite rays

PRI-P05 (Montelli et al., 2006)
90K finite frequency measurements with 20 s dominant period
1.5M short-period traveltimes from bulletins

High-velocity structure at the Core-Mantle Boundary

This study

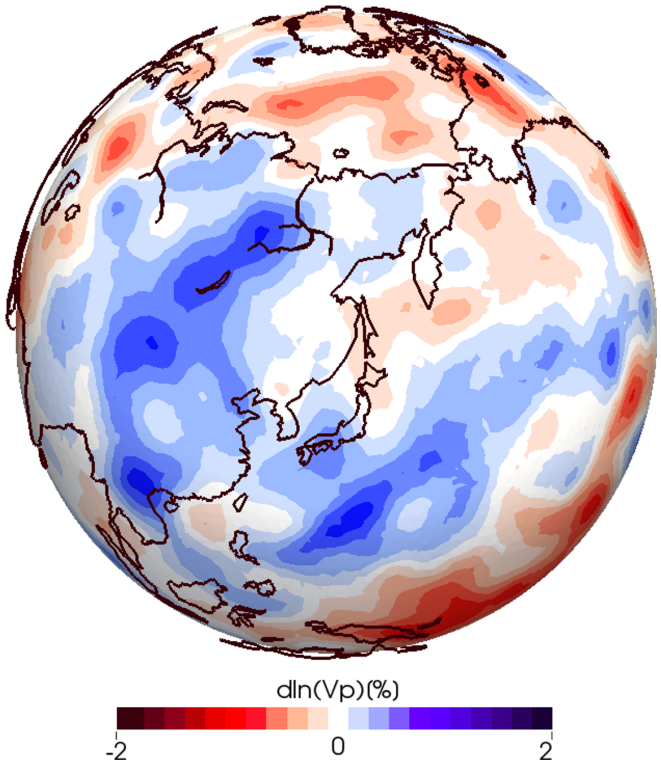

MIT-P08

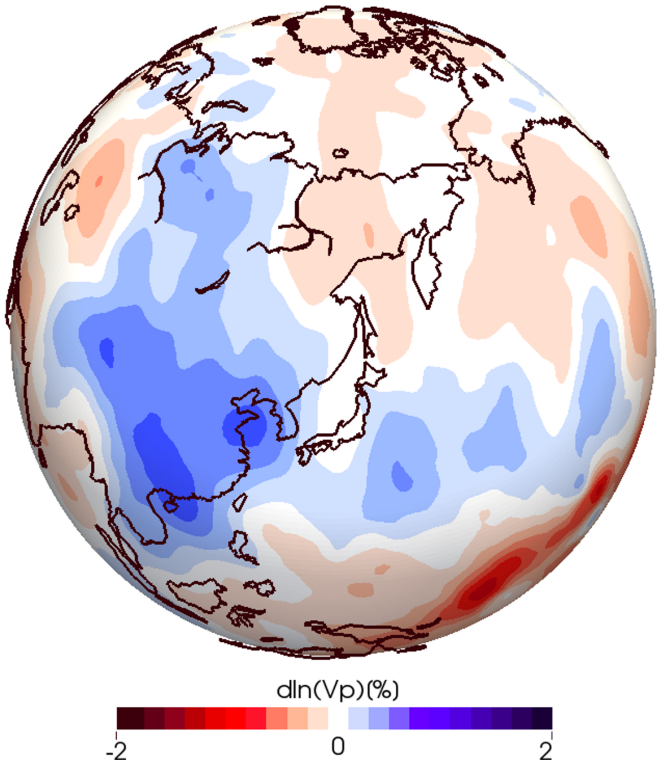

Associated with the remnants of ancient subducted slabs (e.g., Sengör et al., 1993; Fukao et al., 1992; Van der Voo et al., 1999)

Slabs appear as narrower, more linear belts.

High-velocity structure at the Core-Mantle Boundary

This study

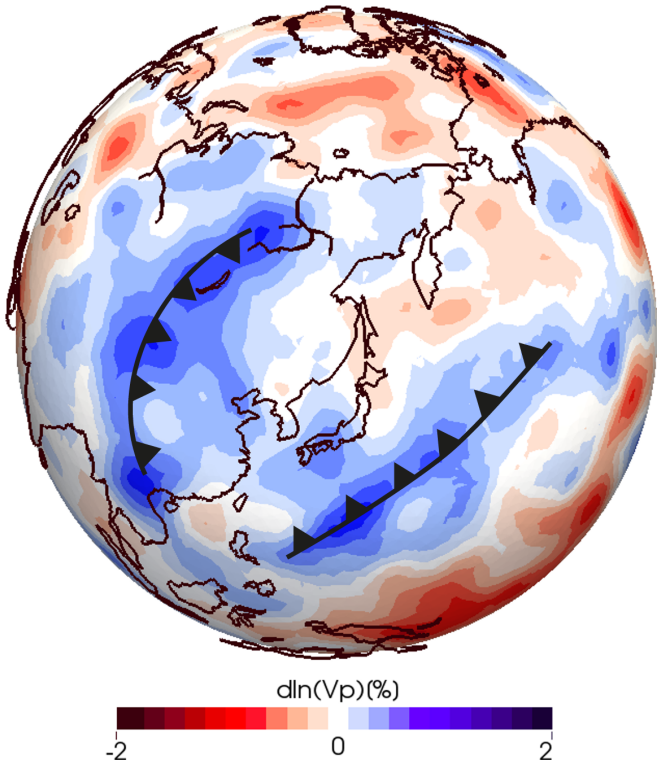

MIT-P08

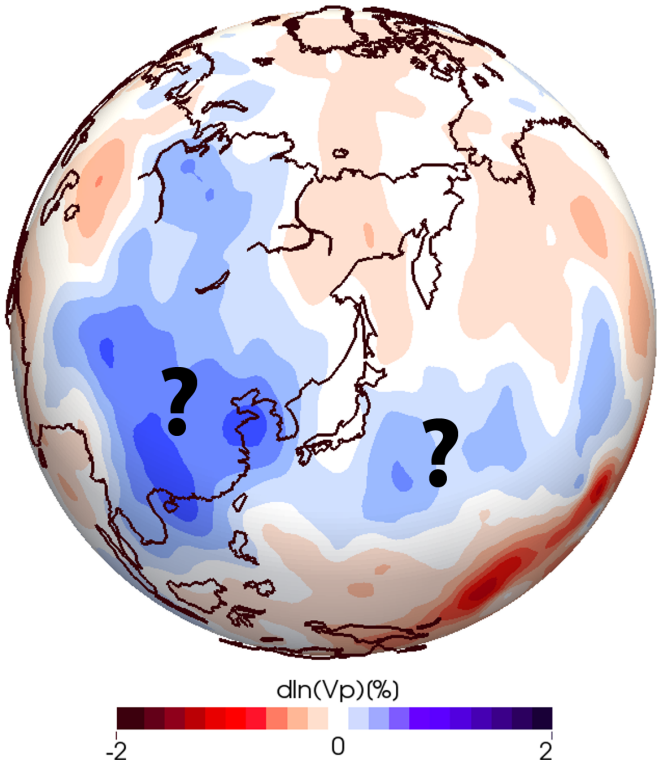

Associated with the remnants of ancient subducted slabs (e.g., Sengör et al., 1993; Fukao et al., 1992; Van der Voo et al., 1999)

Slabs appear as narrower, more linear belts.

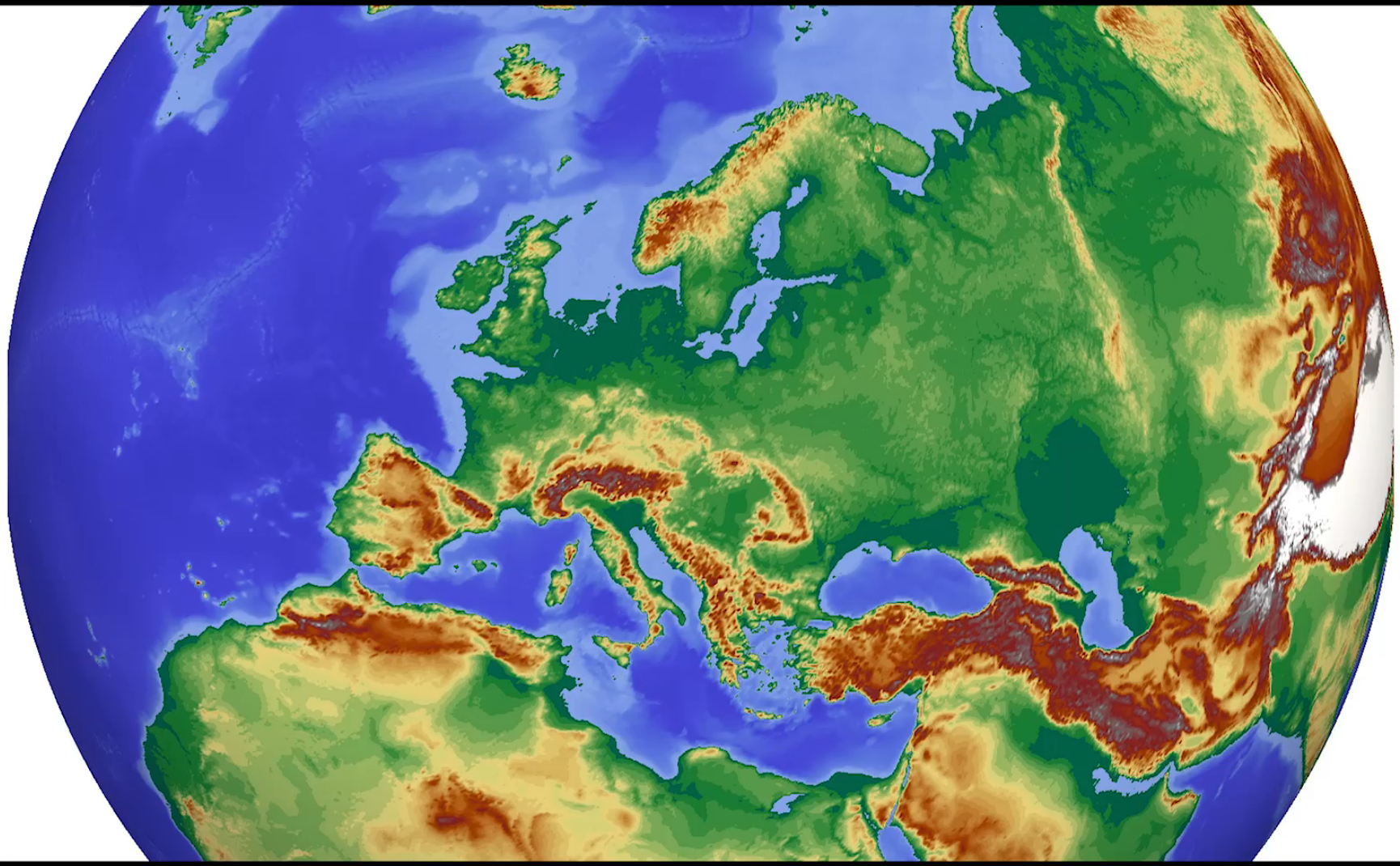

Vote-maps (2850km depth)

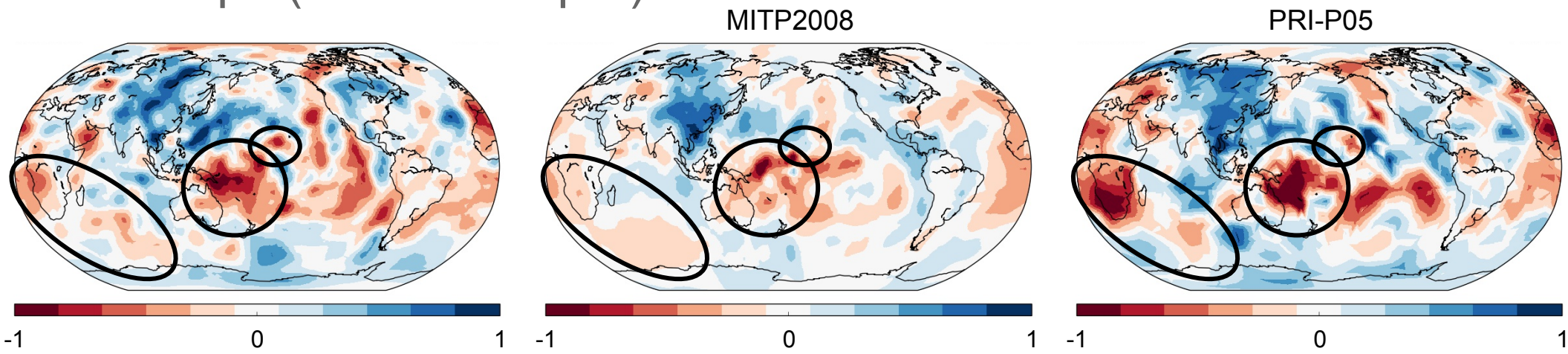

Vote-maps (2850km depth)

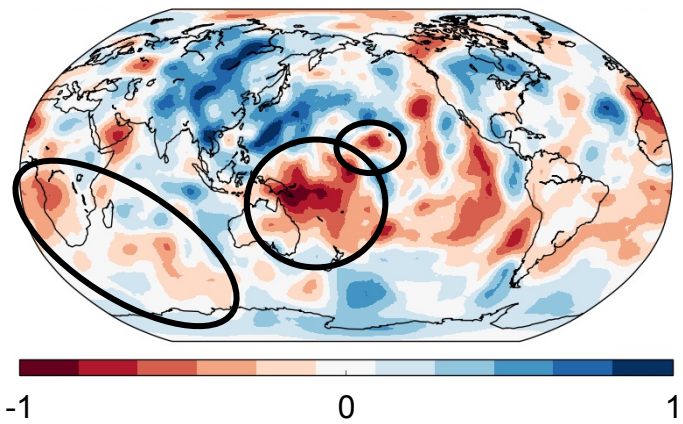

MITP2008

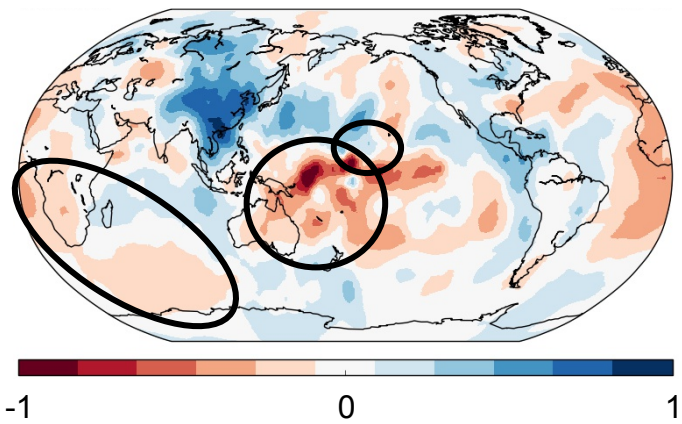

PRI-P05

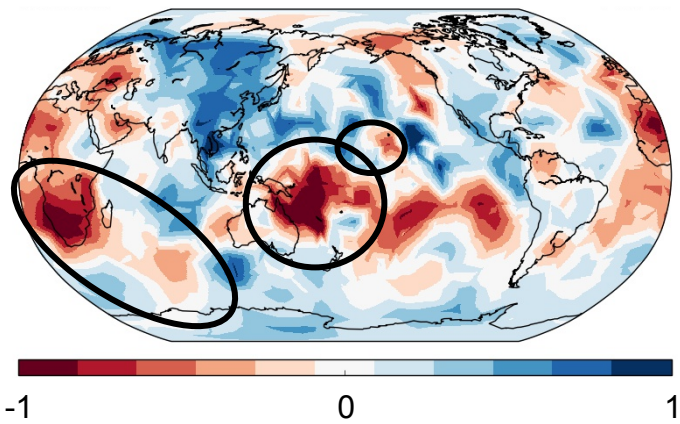

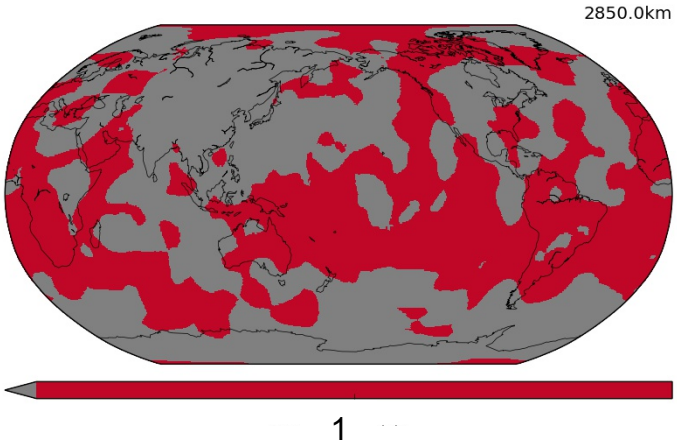

Vote-maps (2850km depth)

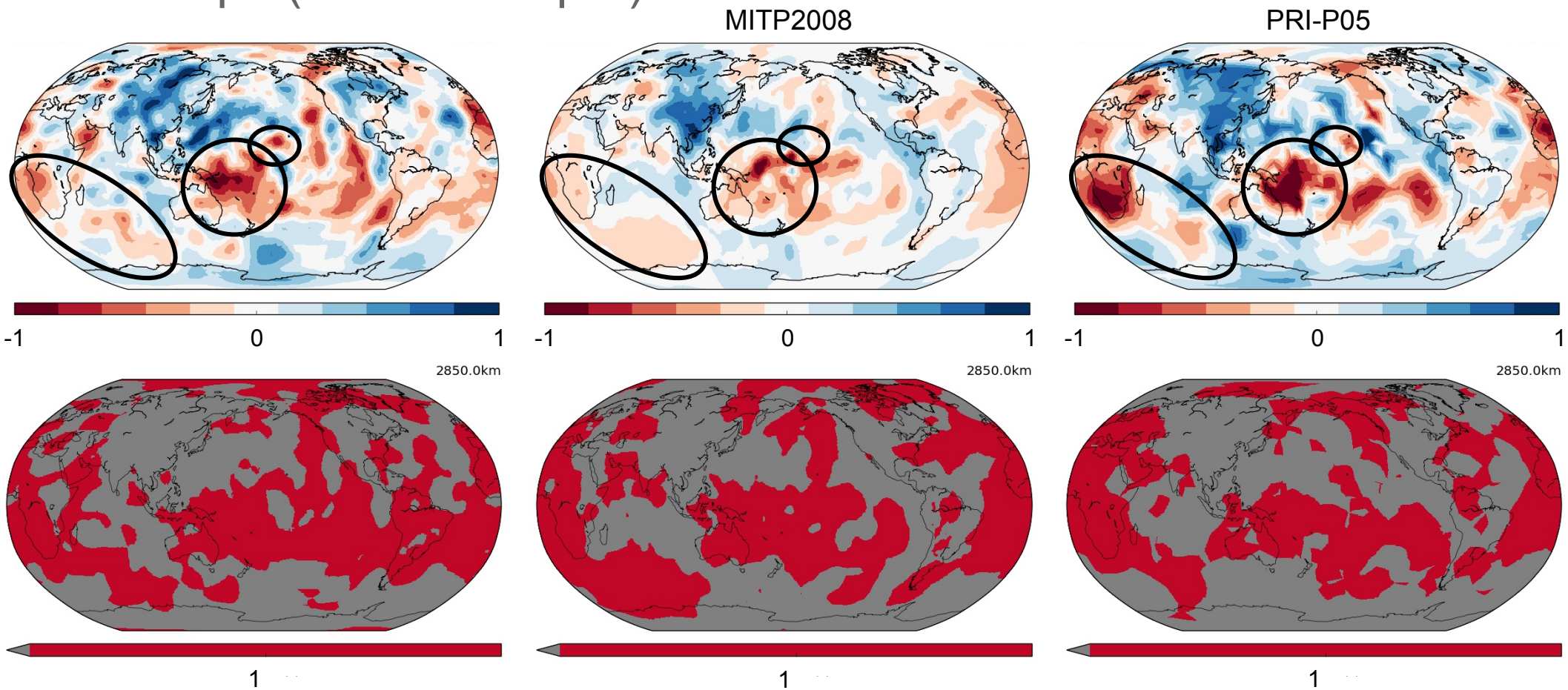

Vote-maps (2850km depth)

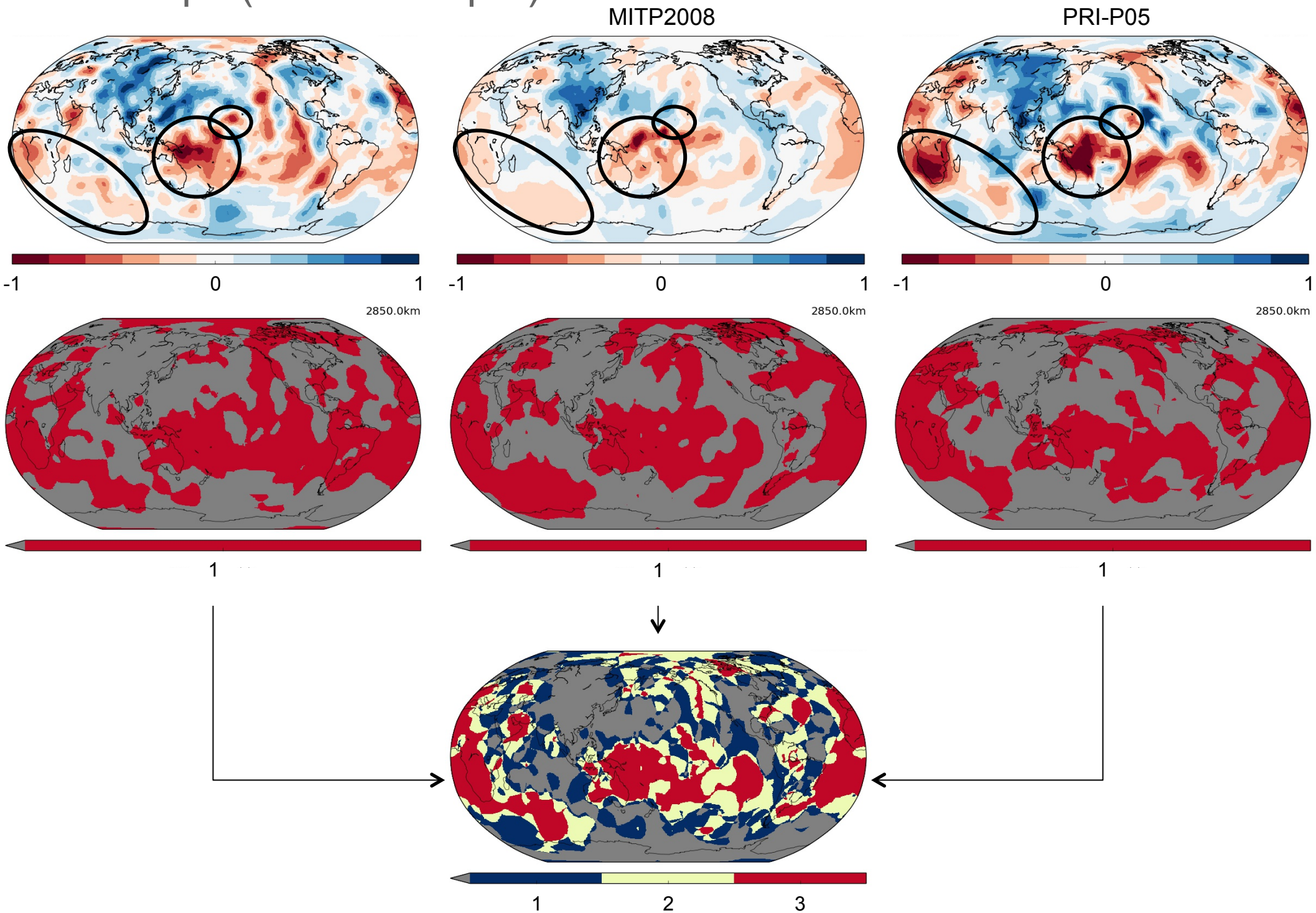

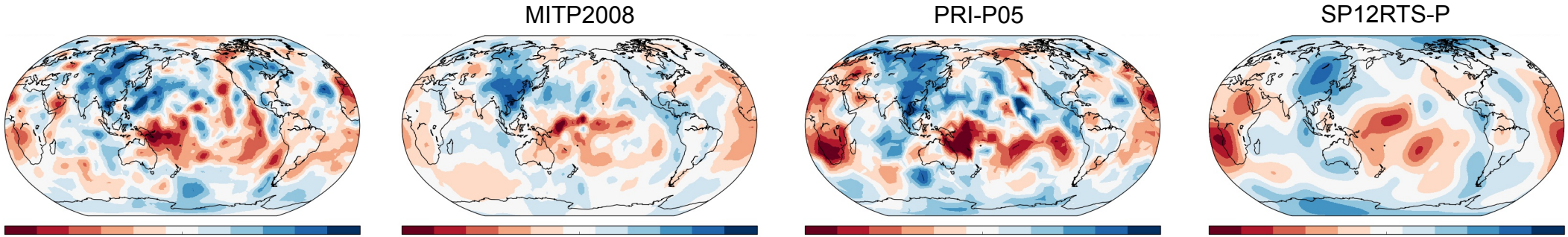
MITP2008
PRI-P05
SP12RTS-P

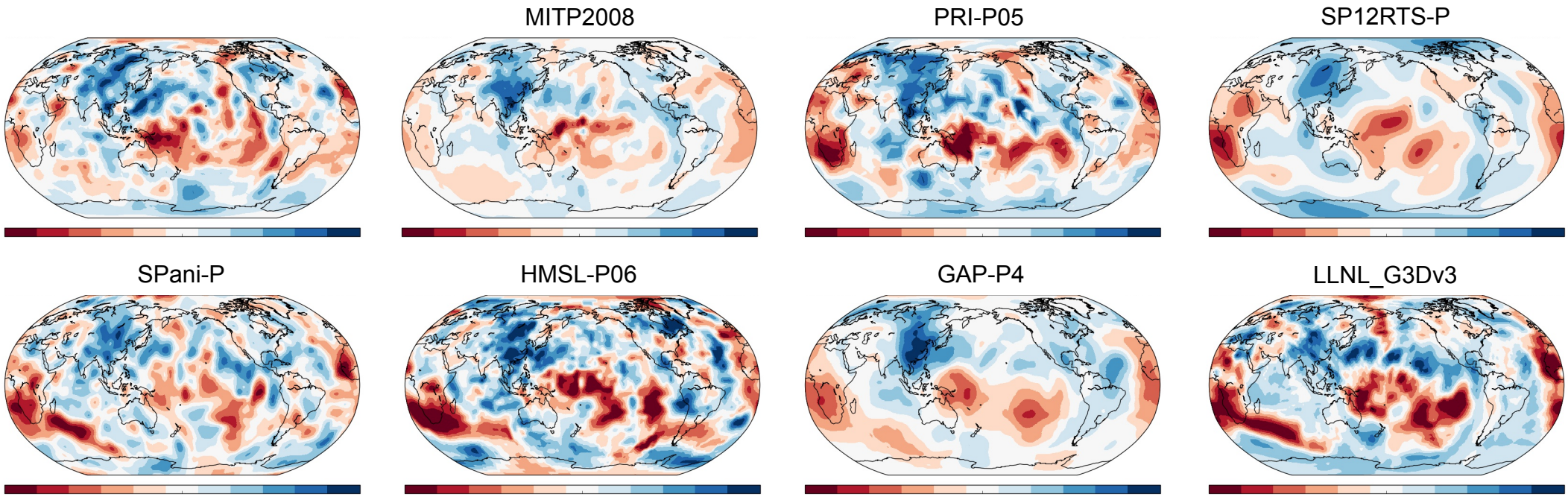
MITP2008
PRI-P05
SP12RTS-P
SPani-P
HMSL-P06
GAP-P4
LLNL_G3Dv3

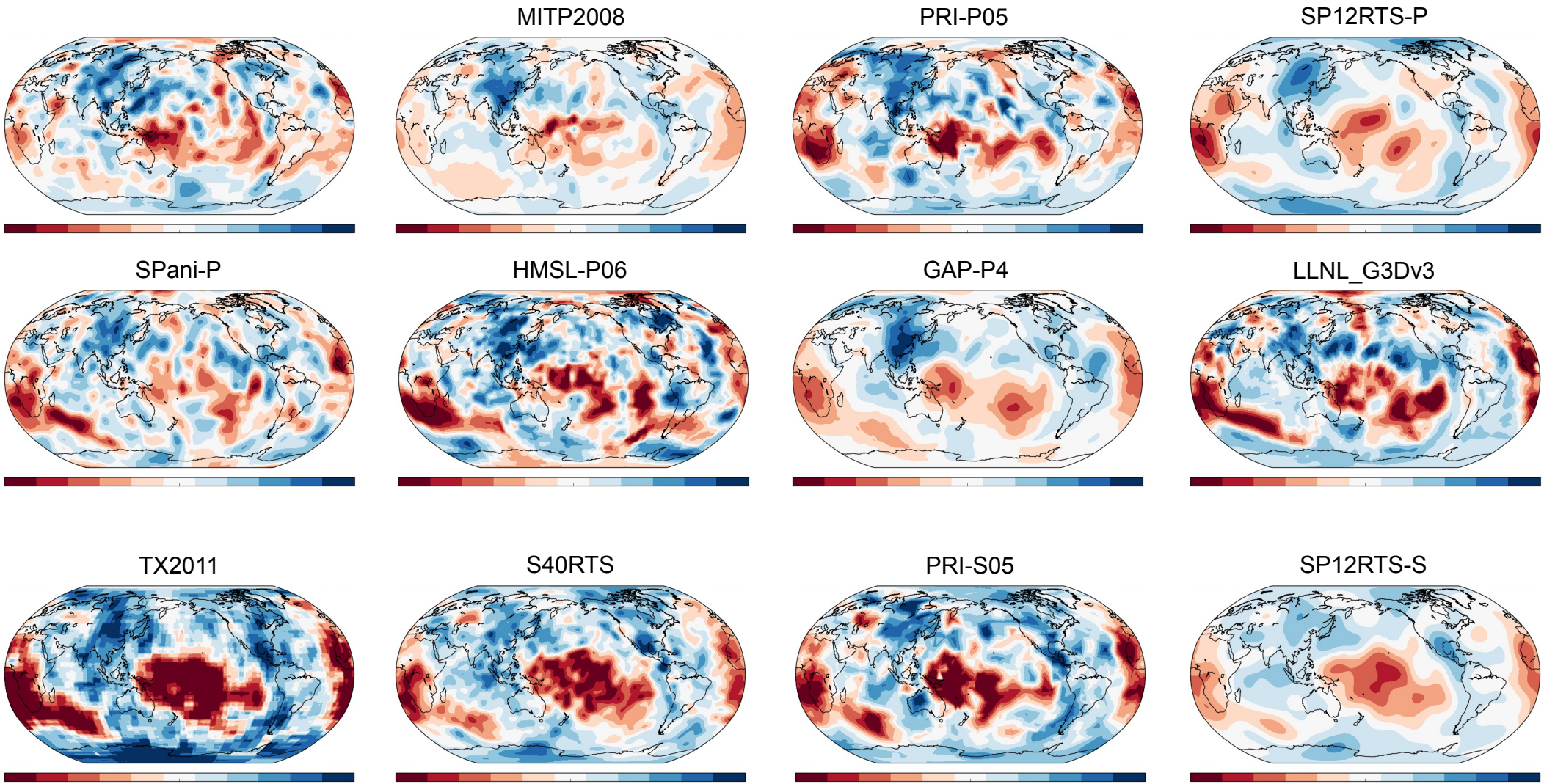
MITP2008
PRI-P05
SP12RTS-P
SPani-P
HMSL-P06
GAP-P4
LLNL_G3Dv3
TX2011
S40RTS
PRI-S05
SP12RTS-S

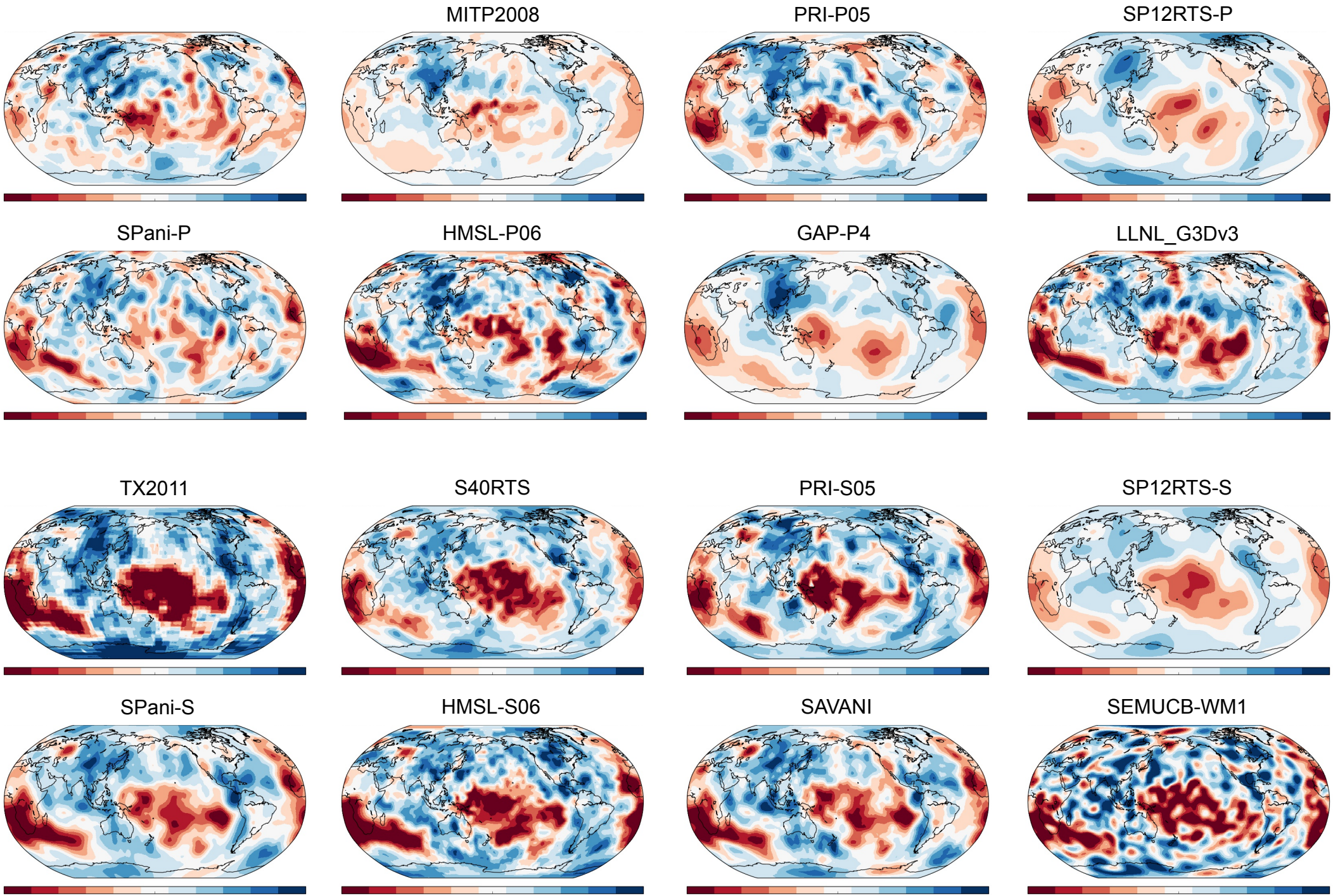
MITP2008
PRI-P05
SP12RTS-P
SPani-P
HMSL-P06
GAP-P4
LLNL_G3Dv3
TX2011
S40RTS
PRI-S05
SP12RTS-S
SPani-S
HMSL-S06
SAVANI
SEMUCB-WM1

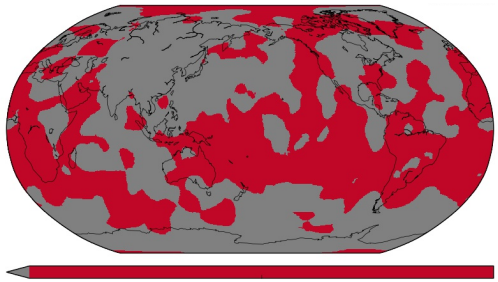

MITP2008

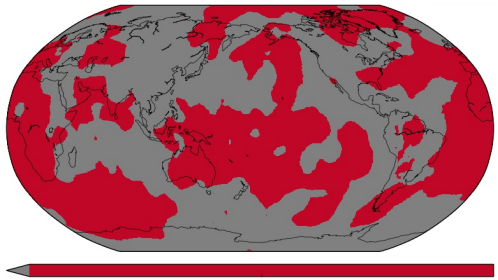

PRI-P05

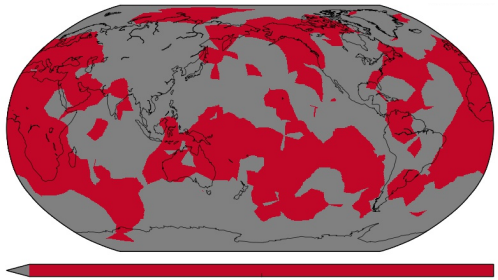

SP12RTS-P

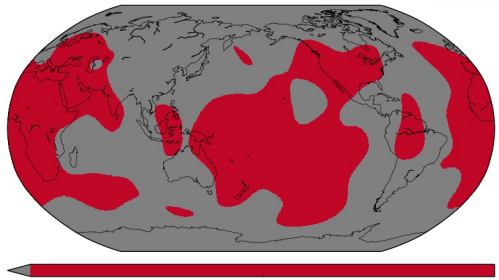

SPani-P

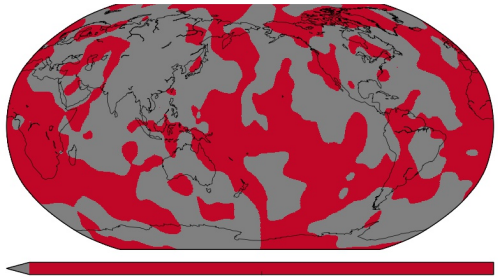

HMSL-P06

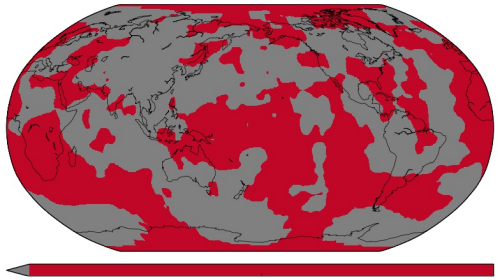

GAP-P4

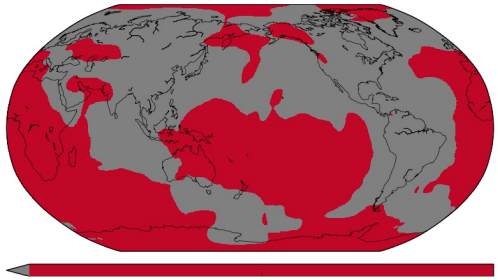

LLNL_G3Dv3

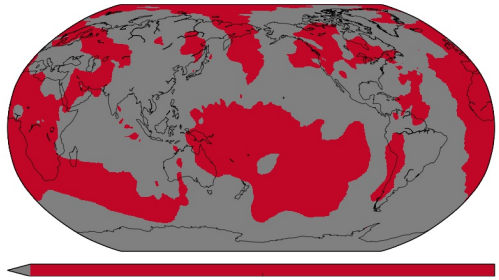

TX2011

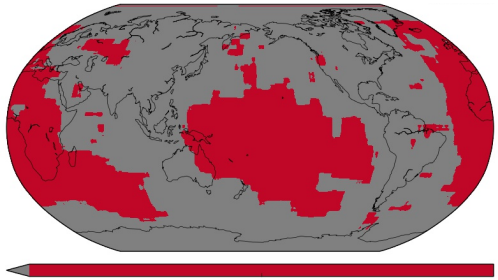

S40RTS

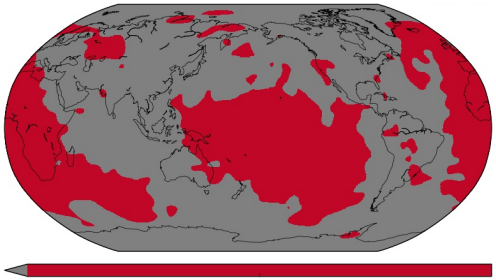

PRI-S05

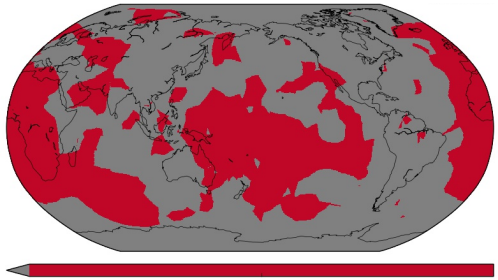

SP12RTS-S

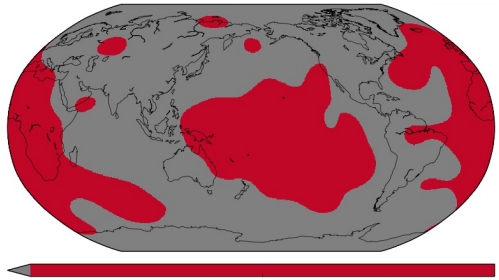

SPani-S

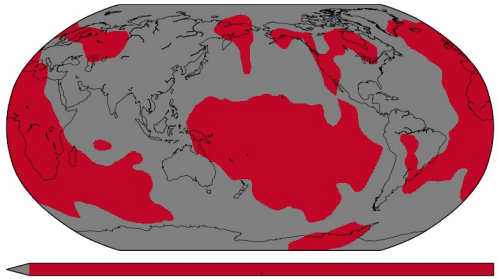

HMSL-S06

SAVANI

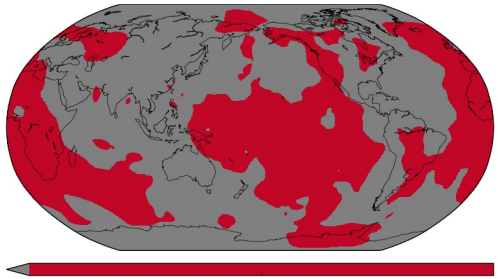

SEMUCB-WM1

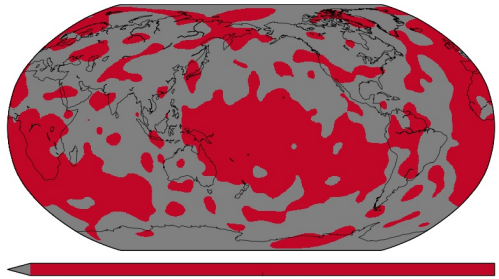

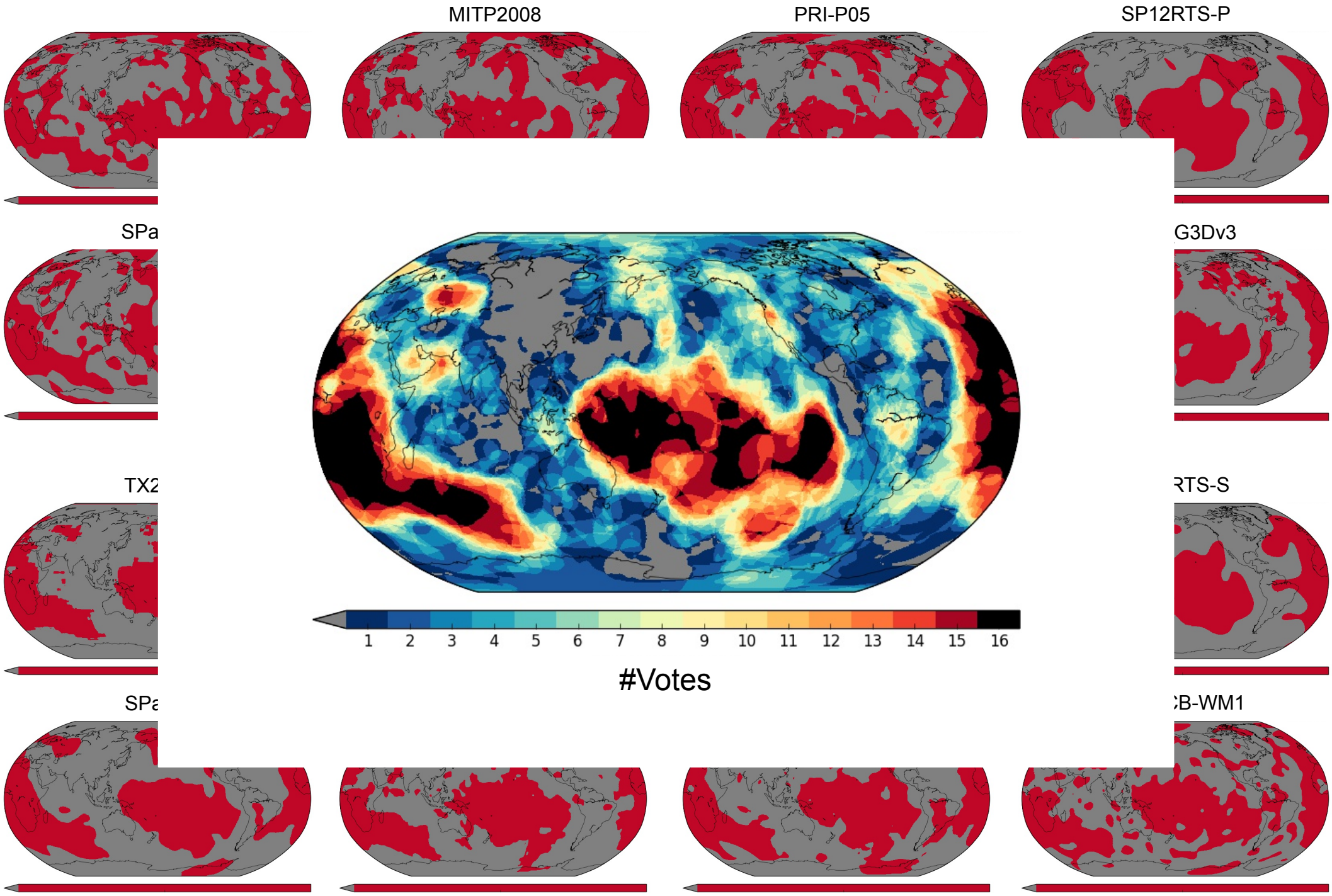
MITP2008
PRI-P05
SP12RTS-P
SPa
G3Dv3
TX2
RTS-S
SPa
B-WM1
1 2 3 4 5 6 7 8 9 10 11 12 13 14 15 16
#Votes

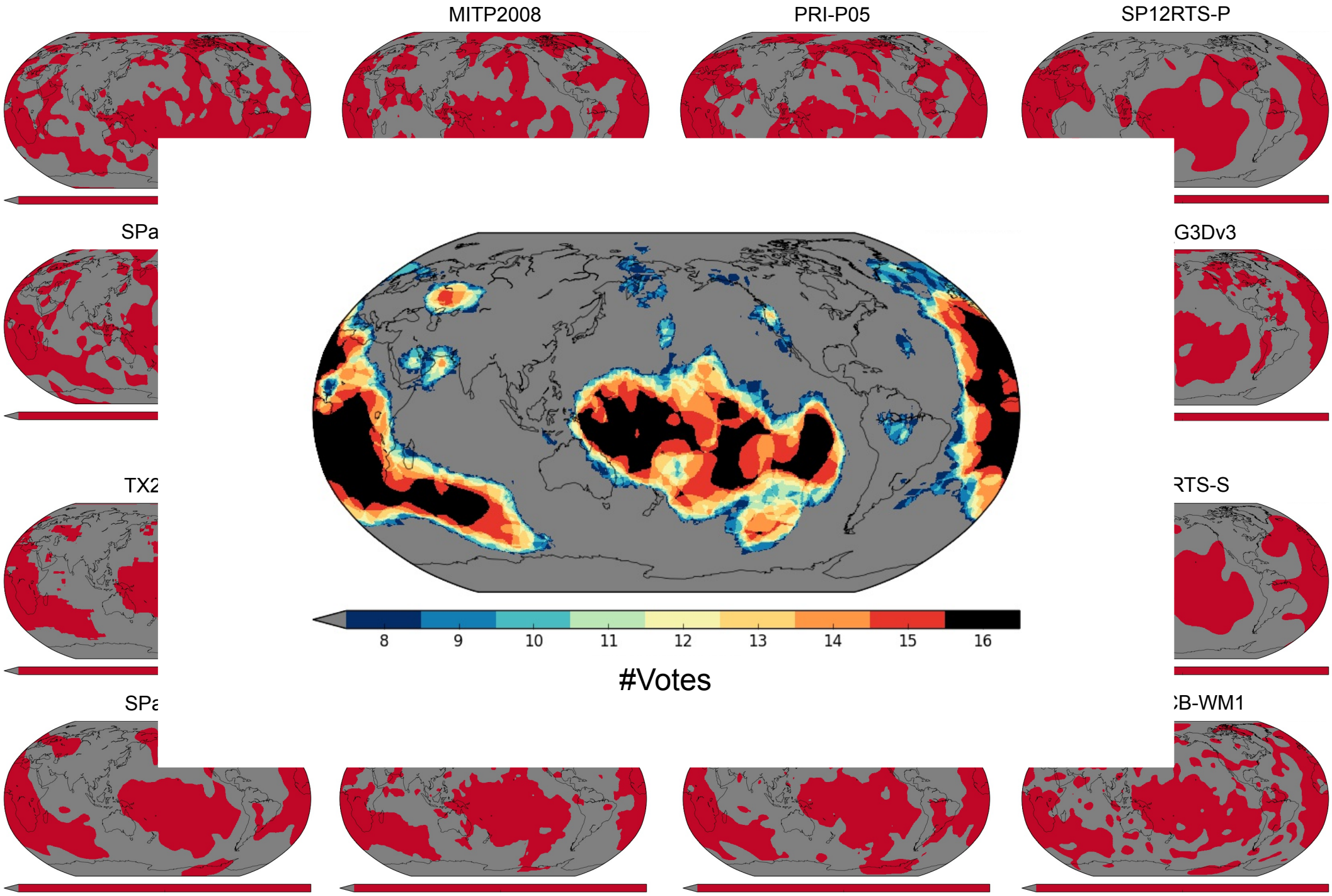
MITP2008
PRI-P05
SP12RTS-P
SPa
G3Dv3
TX2
RTS-S
SPa
B-WM1
8
9
10
11
12
13
14
15
16
#Votes

Web-based tools for interrogating Earth's deep interior

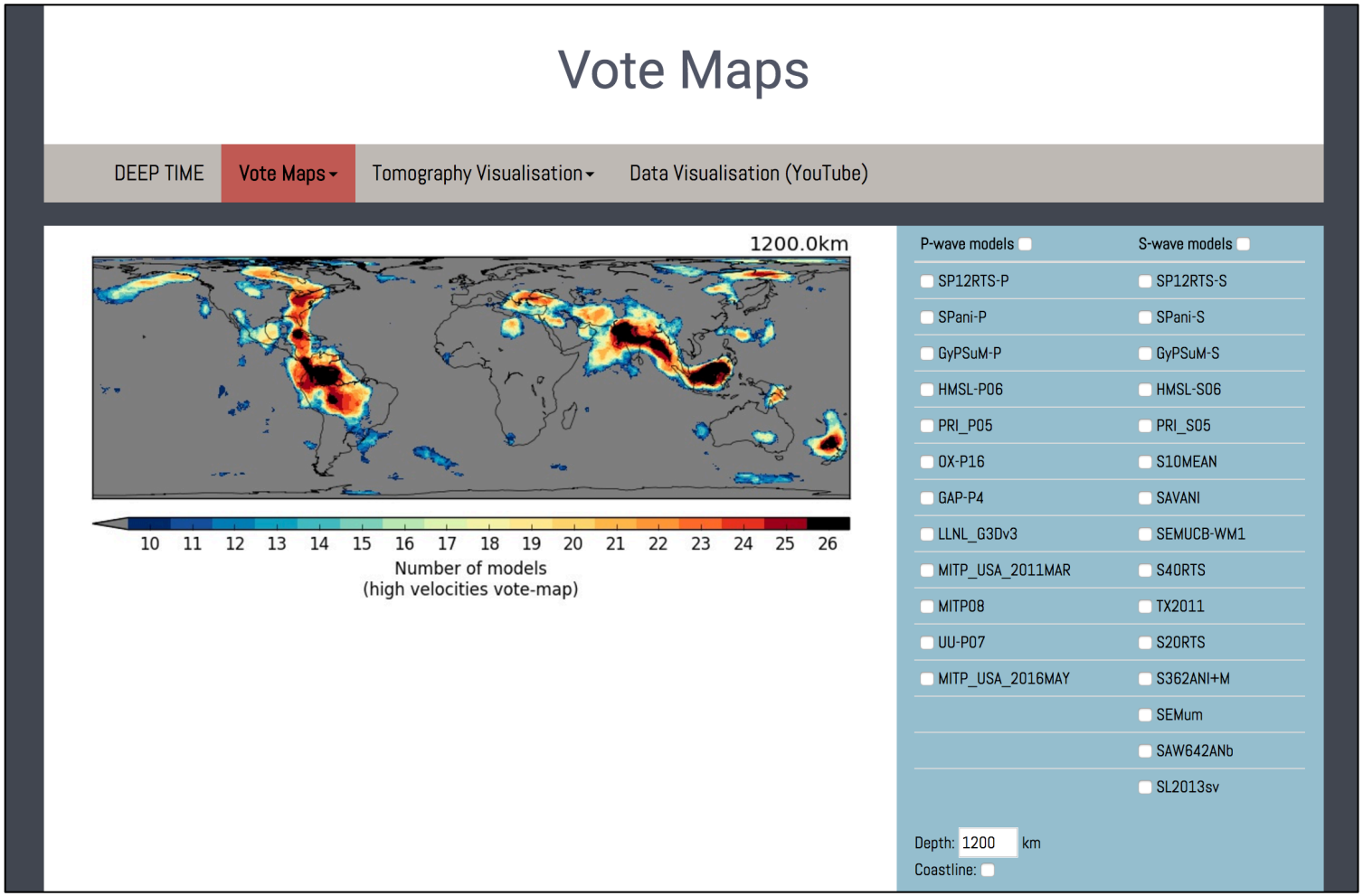

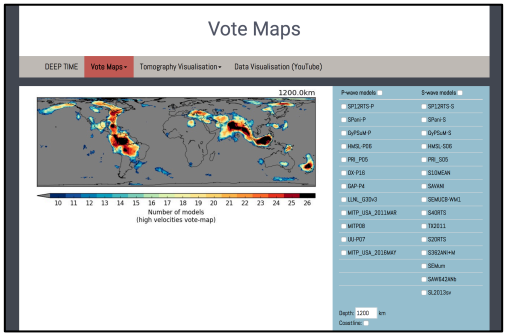
Vote Maps
DEEP TIME
Vote Maps
Tomography Visualisation
Data Visualisation (YouTube)
1200.0km
10 11 12 13 14 15 16 17 18 19 20 21 22 23 24 25 26
Number of models
(high velocities vote-map)
P-wave models
SP12RTS-P
SPani-P
GyPSuM-P
HMSL-P06
PRI_P05
GX-P16
GAP-P4
LLNL_G3Dv3
MITP_USA_2011MAR
MITP08
UU-P07
MITP_USA_2016MAY
S-wave models
SP12RTS-S
SPani-S
GyPSuM-S
HMSL-S06
PRI_S05
S10WDAN
SAVANI
SEMUCB-WM1
S40RTS
TX2011
S20RTS
S362ANI+M
SEMum
SAWE42MN
SL2013sv
Depth: 1200 km
Coastline:

Tomography models (~30 models)

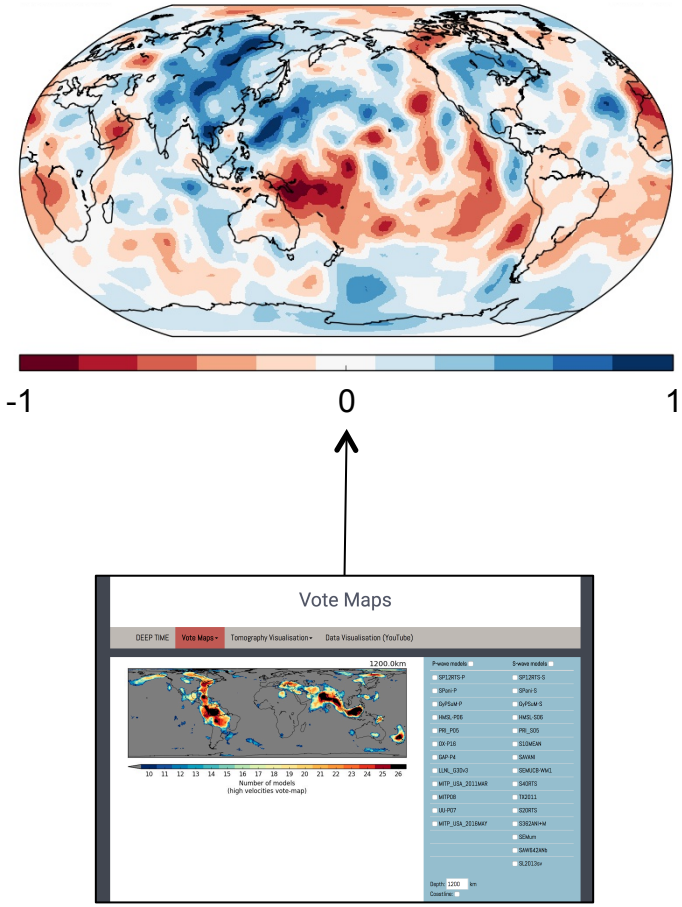

Tomography models (~30 models)

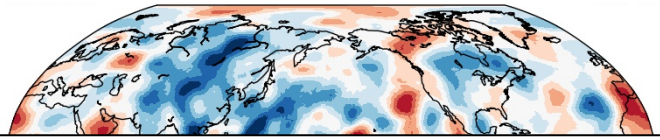

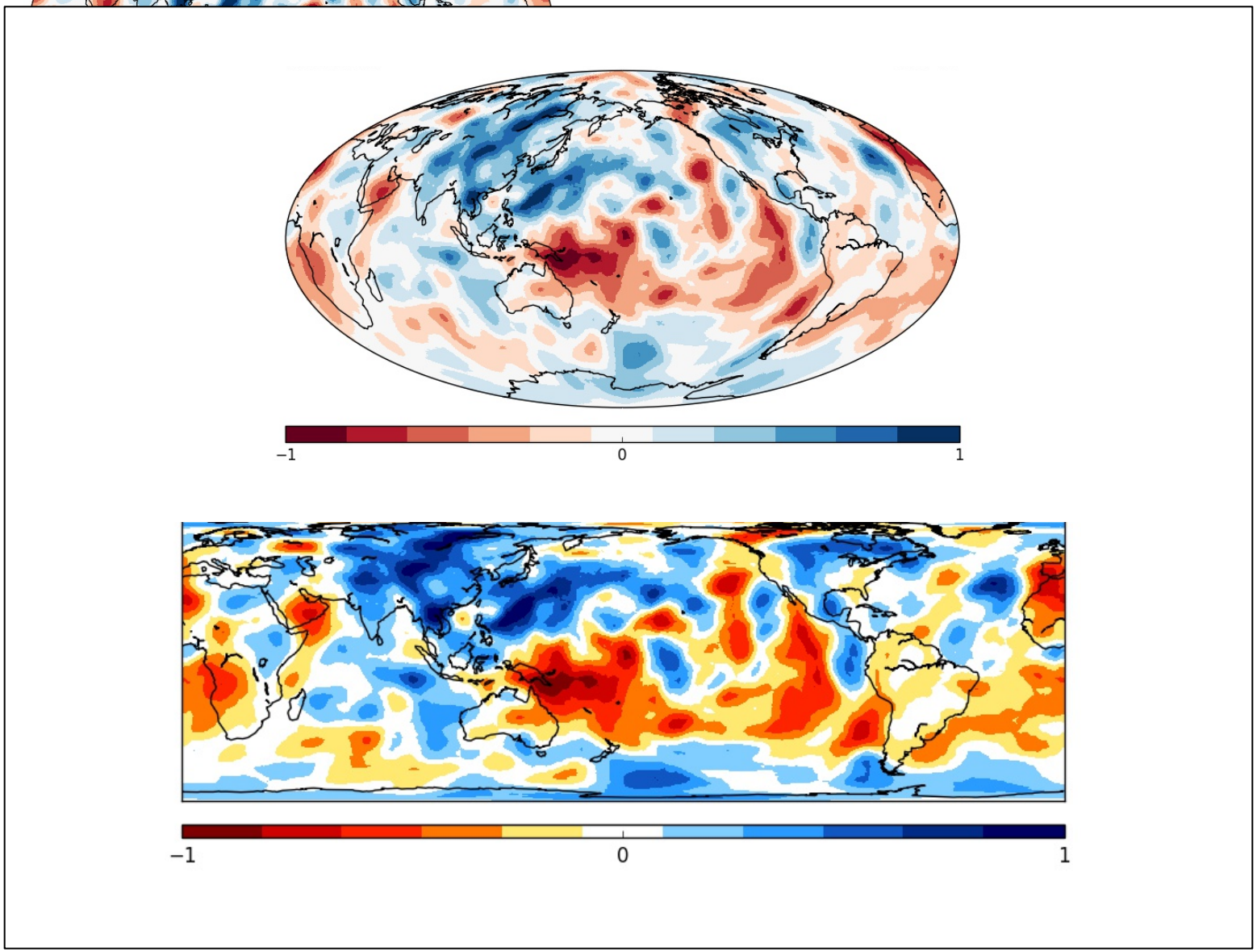

Tomography models (~30 models)

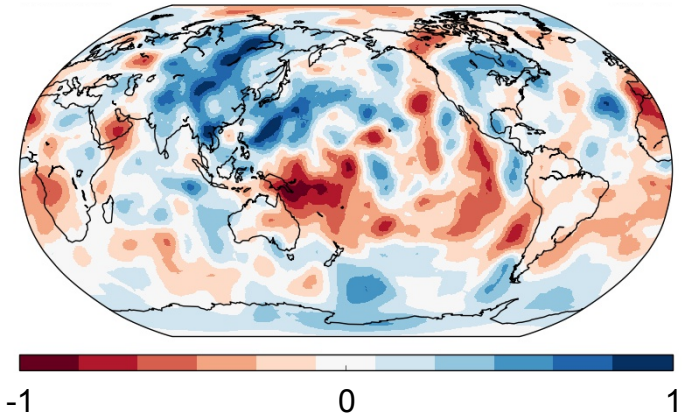

vote-maps

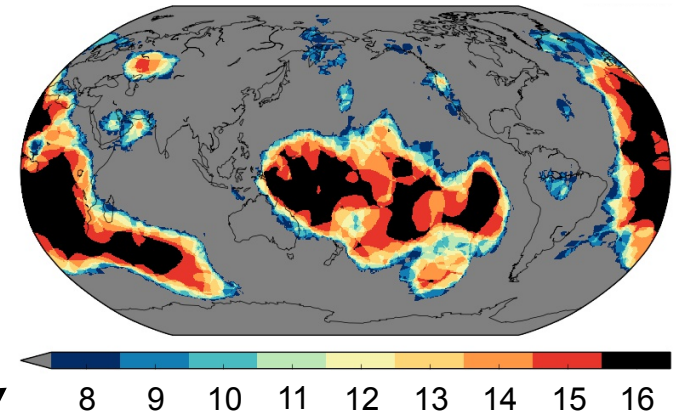

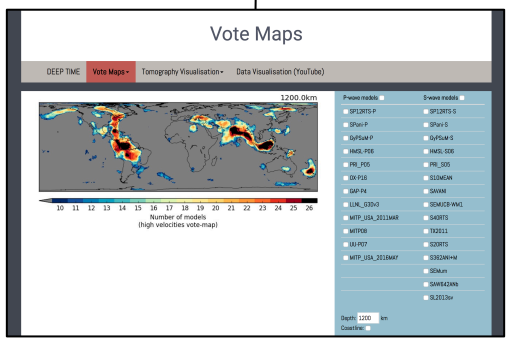

Tomography models (~30 models)

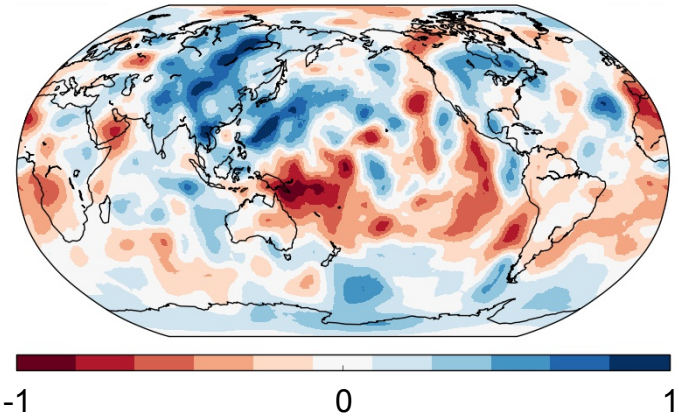

vote-maps

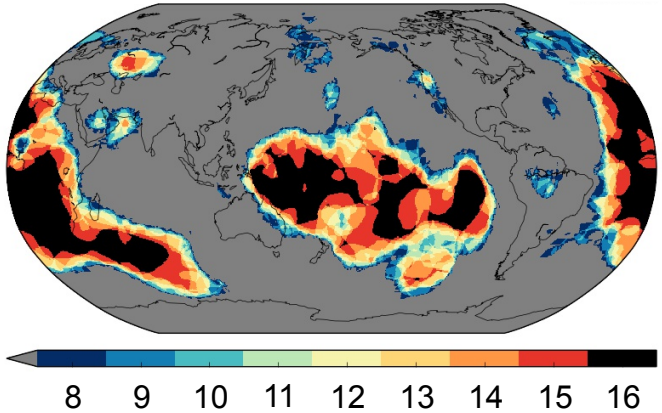

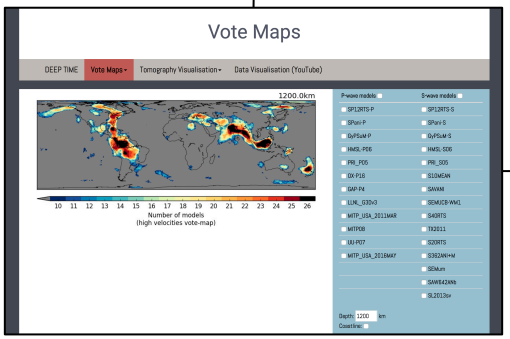

Splitting function (Normal mode)

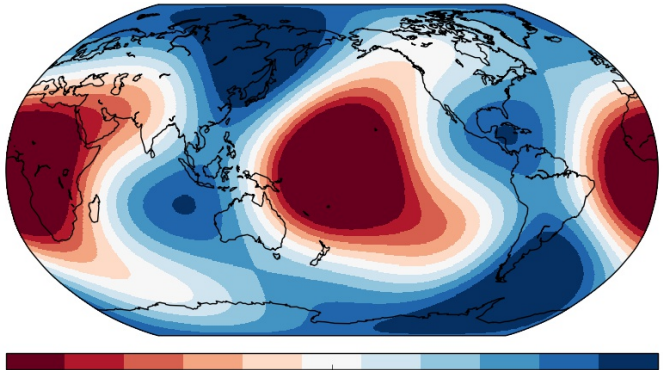

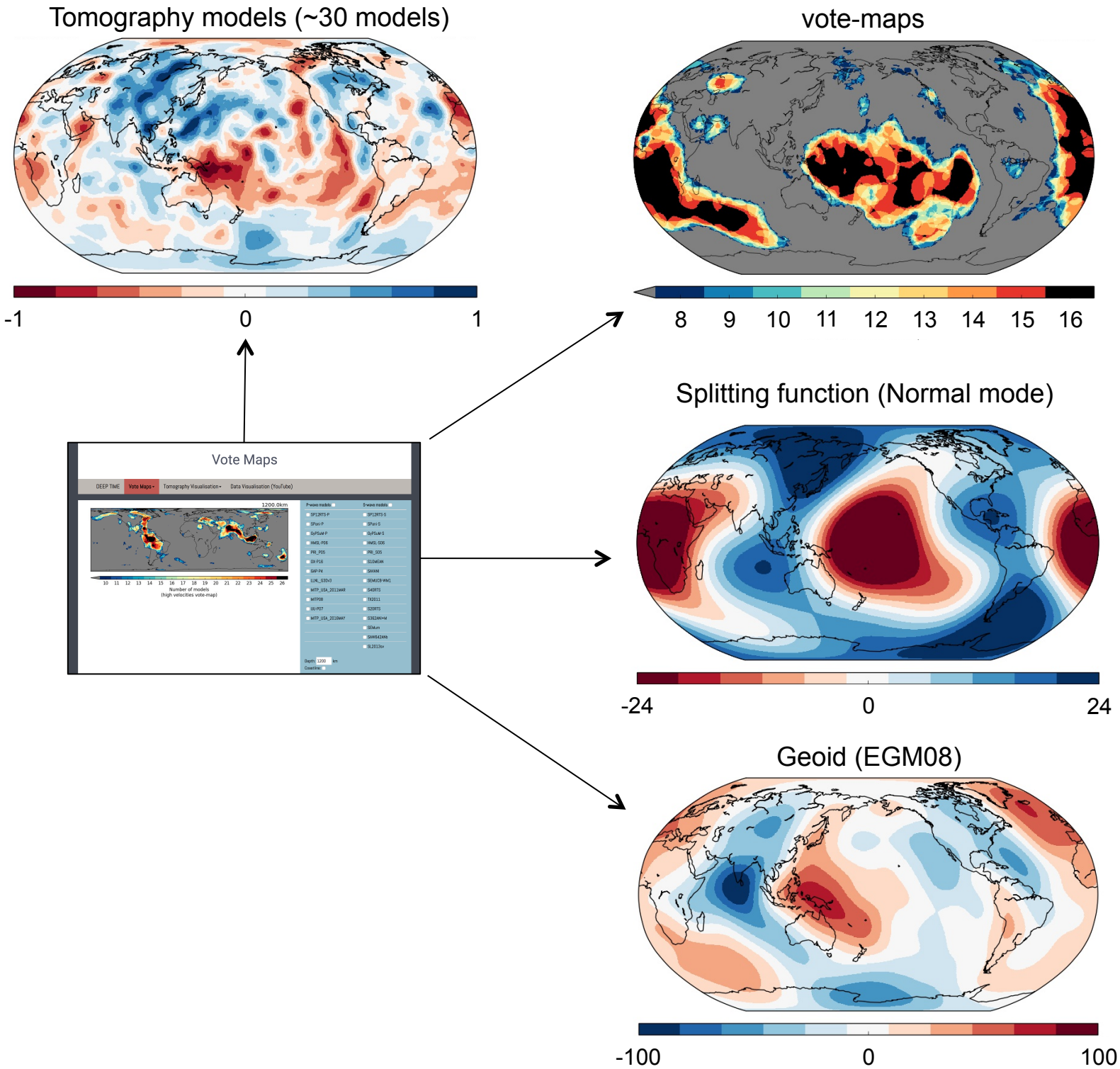
Tomography models (~30 models)
-1
0
1
vote-maps
8
9
10
11
12
13
14
15
16
Vote Maps
DEEP TIME
Vote Maps
Tomography Visualisation
Data Visualisation (YouTube)
1200.0km
Number of models
(high velocities vote-map)
Splitting function (Normal mode)
-24
0
24
Geoid (EGM08)
-100
0
100

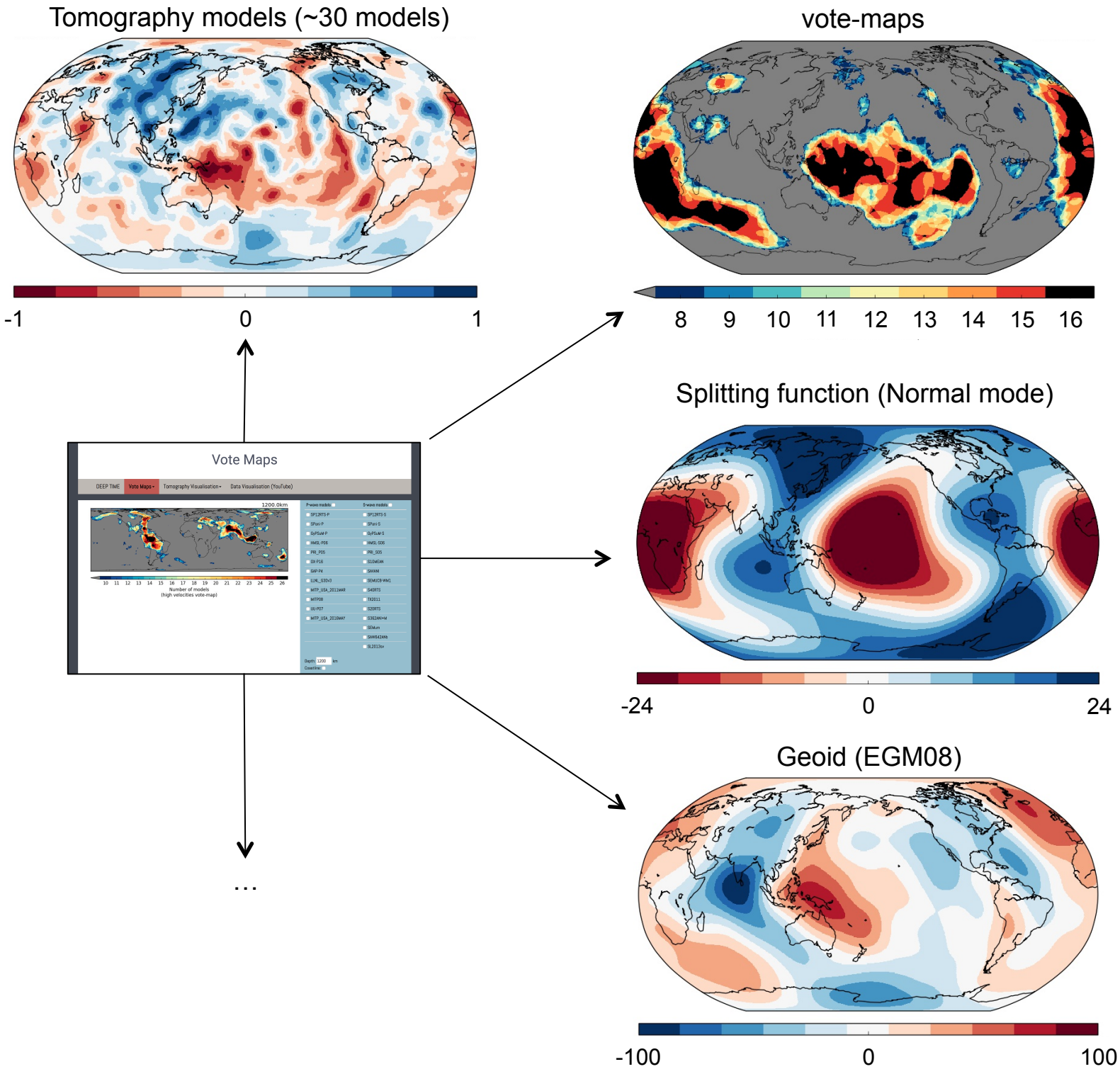
Tomography models (~30 models)
-1
0
1
vote-maps
8
9
10
11
12
13
14
15
16
Vote Maps
DEEP TIME
Vote Maps
Tomography Visualisation
Data Visualisation (YouTube)
1200.0km
Number of models
(high velocities vote-map)
Splitting function (Normal mode)
-24
0
24
Geoid (EGM08)
-100
0
100
...

Tomography models (~30 models)

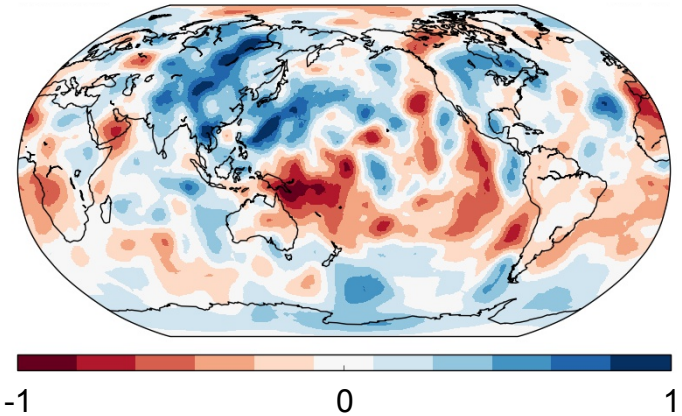

vote-maps

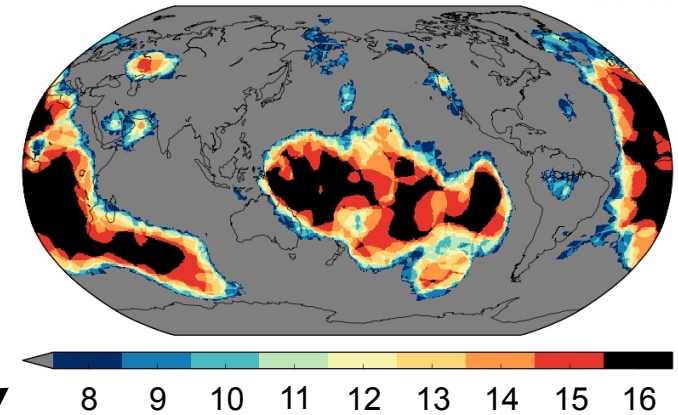

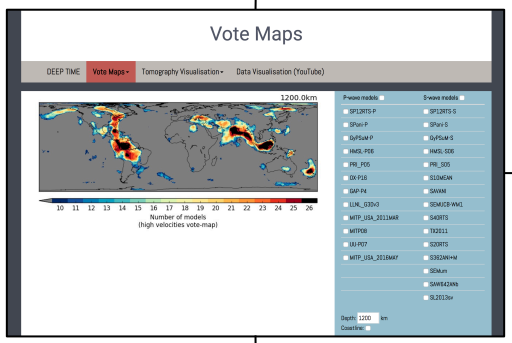

Splitting function (Normal mode)

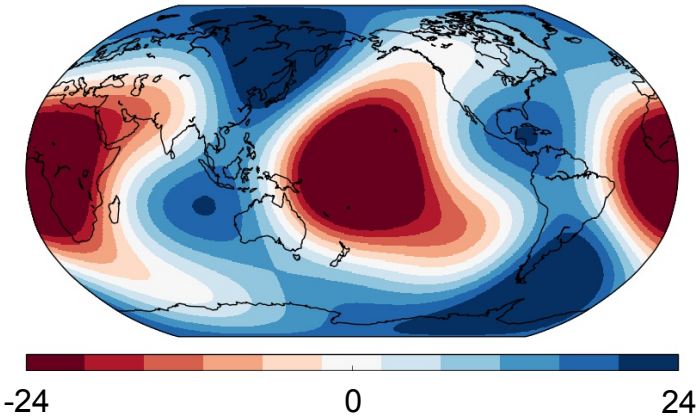

Geoid (EGM08)

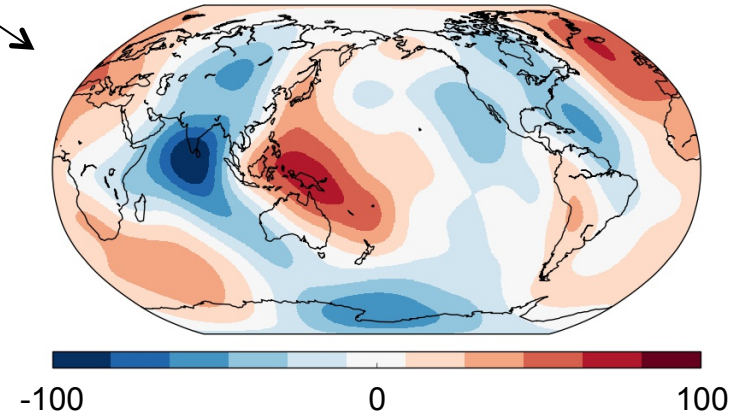

…

Thank You!